

**A PRELIMINARY INVESTIGATION OF THE EFFECTS OF
ENVIRONMENTALLY ASSISTED CRACKING ON NATURAL GAS
TRANSMISSION PIPELINES**

A Thesis

by

JASON WAYNE CURBO

Submitted to the Office of Graduate Studies of
Texas A&M University
in partial fulfillment of the requirements for the degree of
MASTER OF SCIENCE

May 2005

Major Subject: Mechanical Engineering

**A PRELIMINARY INVESTIGATION OF THE EFFECTS OF
ENVIRONMENTALLY ASSISTED CRACKING ON NATURAL GAS
TRANSMISSION PIPELINES**

A Thesis

by

JASON WAYNE CURBO

Submitted to Texas A&M University
in partial fulfillment of the requirements
for the degree of

MASTER OF SCIENCE

Approved as to style and content by:

Richard Griffin
(Chair of Committee)

Harry Hogan
(Member)

David Trejo
(Member)

Dennis O'Neal
(Head of Department)

May 2005

Major Subject: Mechanical Engineering

ABSTRACT

A Preliminary Investigation of the Effects of Environmentally Assisted Cracking on
Natural Gas Transmission Pipelines. (May 2005)
Jason Wayne Curbo, B.S., University of Arkansas
Chair of Advisory Committee: Dr. Richard Griffin

Concepts for the development of a model to predict natural gas transmission pipeline lifetime in a corrosive environment are constructed. Primarily, the effects of environmentally assisted cracking (EAC) are explored. Tensile test specimens from a sample of API 5L X-52 pipeline were tested in a simulated groundwater solution and subsequently analyzed. The results suggested that the simulated environment ultimately reduced the ductility of the test specimens; however, no evidence of “classical” stress corrosion crack morphology was discovered. However, corrosion pits up to 0.75 mm (0.03 in) were revealed during metallographic analysis. A Marin factor analogy and an energy method concept are suggested and explored. Ultimately, the test data set was too small for the results to be of any directly applicable significance.

ACKNOWLEDGEMENTS

The author would like to acknowledge that all environmental scanning electron microscope images were obtained on equipment purchased under National Science Foundation grant #ECS-9214314. Above all, my friends and family are applauded for their endless patience and support.

TABLE OF CONTENTS

	Page
ABSTRACT	iii
ACKNOWLEDGEMENTS	iv
TABLE OF CONTENTS	v
LIST OF FIGURES.....	vii
LIST OF TABLES	x
INTRODUCTION.....	1
FUNDAMENTALS OF ENVIRONMENTALLY ASSISTED CRACKING.....	3
Stress Corrosion Cracking.....	4
Corrosion Fatigue Cracking	8
Hydrogen Induced Cracking	10
STRESS CORROSION CRACKING MECHANISM	13
Slip Dissolution / Film Rupture Model	13
Stable Oxide Film and Crack Initiation.....	16
PIPELINE MATERIAL	20
ENVIRONMENTAL CONSIDERATIONS.....	22
Carbonate / Bicarbonate	22
EXPERIMENTATION	27
Theory	27
Experimental Description.....	30
Equipment and Setup	31
Test Specimens.....	32
EXPERIMENTAL RESULTS AND DISCUSSION.....	34

	Page
CERT Test Results	34
Visual Inspection.....	40
Scanning Electron Microscopy	46
Energy Dispersive Spectroscopy.....	55
Metallographic Analysis	61
Marin Factor Analogy	64
Strain Energy Concept	68
APPLICATION TO PIPELINE LIFETIME AND FUTURE RESEARCH.....	73
CONCLUSION	75
REFERENCES	77
APPENDIX A	79
APPENDIX B	82
VITA	84

LIST OF FIGURES

FIGURE	Page
1 Illustration depicting a corrosion system.	4
2 Propagation rate versus the crack tip stress intensity.	6
3 Potential versus the log of current density.	8
4 Schematic of an SCC mechanism.	14
5 Schematic effect of strain rate on ductility.	16
6 Pourbaix diagram for iron.	17
7 Illustration of the corrosion of iron.	18
8 Schematic of the experimental setup.	31
9 Diagram of the CERT specimen.	32
10 Load / extension curves for each specimen.	36
11 Graph depicting % elongation and % reduction in area.	38
12 Graph depicting fracture and ultimate loads.	39
13 Graph depicting the fracture, ultimate, and breaking stresses.	40
14 Visual inspection of test specimen 1.	41
15 Visual inspection of test specimens 2 and 3.	41
16 Visual inspection of test specimen 4.	42
17 Visible “cracks” on test specimen 4.	43
18 Visual inspection of test specimen 5 – fracture surfaces.	43
19 Visual inspection of test specimen 5 – side views.	44

FIGURE	Page
20 Visual inspection of test specimen 6 – fracture surfaces.....	45
21 Visual inspection of test specimen 6 – side view.....	45
22 SEM images of test specimens 1 and 4.....	46
23 SEM images of test specimens 2 and 5.....	47
24 SEM images of test specimens 3 and 6.....	47
25 SEM image of test specimen 5 after cleaning.....	48
26 SEM images of test specimens 1 and 4 – shear lip.....	49
27 SEM images of test specimens 2 and 5 – shear lip.....	50
28 SEM images of test specimens 3 and 6 – shear lip.....	50
29 SEM images of test specimen 4.....	51
30 SEM image of the fracture surface of test specimen 4.....	52
31 Image of an embrittled portion of test specimen 4 fracture surface.....	53
32 SEM images of test specimen 5.....	54
33 SEM image of test specimen 6.....	54
34 EDS analysis of test specimen 1.....	56
35 EDS analysis of test specimen 2.....	57
36 EDS analysis of test specimen 2 anomaly.....	58
37 EDS analysis of test specimen 4 – corrosion product.....	59
38 EDS analysis of test specimen 4 – near surface.....	60
39 Micrographs from test specimens 1 and 2.....	61
40 Images of pits in the test specimens.....	62

FIGURE	Page
41 Lateral section of X-52 pipeline steel.	63
42 Prediction of specimen lifetime from reduction in area.	65
43 Graph of the generalized ratio prediction.	67
44 Graphic of the difference in energy for tests 1 and 4.	69
45 Graphic of the difference in energy for tests 2 and 5.	70
46 Graphic for the difference in energy for tests 3 and 6.	71
47 Material chemistry data.	80
48 Material mechanical data.	81
49 Graph of calibration data.	83

LIST OF TABLES

TABLE	Page
1 Manufacturer's Chemical Analysis	20
2 API 5L X52 Mechanical Specifications.....	21
3 Subfactor Hierarchy	29
4 Initial Dimensions of the Test Specimens.....	33
5 CERT Data	34
6 CERT Mechanical Results	35
7 % Changes in CERT Data.....	37
8 API 5L Strength Requirements	63
9 Ratio of Corrosive Results and Ambient Results.....	64
10 Test Specimen Lifetime Prediction from Ratios.....	64
11 Root Mean Square Variance	65
12 Lifetime Prediction Matrix.....	66
13 Root Mean Square Variance of the Lifetime Predictions	66

INTRODUCTION

Corrosion related deterioration of wall thickness in natural gas transmission pipelines (NGTP) is a major cause of pipeline damage and overall lifetime reduction. In the period beginning January 1, 1991 and ending December 31, 2002 incidents attributed to corrosion damage resulted in 12 fatalities and expenses totaling \$45,278,020.¹ Such safety hazards and expenses are often unnecessary since corrosion related damage, if detected, can typically be repaired during routine inspections and maintenance.

In general, pipeline maintenance is performed using isochronal (hours of operation), periodic (calendar intervals), as discovered, or alert schedule bases. As such, the area receiving attention may or may not actually need service. For instance, the Office of Pipeline Safety issued an alert notice that all operators with pre-1970 electric resistance welded (ERW) pipe should review, examine, survey, and consider hydrostatic testing.² Certainly, 100% of this type of pipe was not in need of this level of inspection and testing, however, the uncertainty in existing conditions and the lack of an accurate, robust lifetime prediction model necessitated that a general alert be distributed. If the existing condition of NGTP's can be characterized and combined with a comprehensive lifetime prediction model, then the need for such "blanket" recommendations could be reduced. Such a model would be instrumental in shifting the current maintenance paradigm into a more economically efficient program.

Corrosion is by general definition the destructive result of an electro-chemical reaction between a metal and its environment. Existing in numerous forms, corrosion

¹This thesis follows the style and format of Corrosion Science.

and its kinetics cannot currently be accurately described by any one single model. Past approaches in pipeline lifetime prediction in the Department of Mechanical Engineering at Texas A&M University include the development of a uniform corrosion growth rate model. A deterministic approach was adapted from procedures developed by the Electric Power Research Institute and used to evaluate the remaining strength of a corroded pipeline. Ultimately, three levels of increasing complexity were used to assess the remaining lifetime of the equipment.³ Continuing in the same spirit, the focus of this thesis is the initial development of a model describing the lifetime of a NGTP subject to environmentally assisted cracking (EAC).

FUNDAMENTALS OF ENVIRONMENTALLY ASSISTED CRACKING

EAC is a general term for brittle mechanical failures resulting from a synergism between tensile stress and a corrosive environment. In the absence of the tensile stress, the specific corrosive environment will typically produce a very slow corrosion growth rate.⁴ However, the combination of a susceptible material, tensile stress, and environment is capable of resulting in EAC.

Essentially, EAC is a spectrum of various forms of corrosion including stress corrosion cracking (SCC), corrosion fatigue cracking (CFC), and hydrogen embrittlement or hydrogen induced cracking (HIC).⁵

The stress may be applied, residual, or a combination of both. The effects of residual stresses can result in the failure of a pipeline even when applied stresses are well below the specified minimum yield strength (SMYS) of the pipe material. Recent research also suggests that pressure fluctuations may be required for crack initiation and growth.⁶

The resultant cracking may be intergranular (between grains), transgranular (across grains), or both; however, the crack path is always normal to the tensile component of stress. Transgranular failures are less common and typically propagate across grains on specific crystal planes, e.g., {100}, {110}, and {210}.⁵ The mode of failure also appears brittle in nature, even when the base material is normally ductile. Failures of this type can be particularly insidious because there is usually no manifestation of a problem before cracking appears.⁴ Complicating matters further, magnetic flux leakage inspections are incapable of locating these cracks.⁷

Stress Corrosion Cracking

Stress corrosion cracking (SCC) is the brittle failure of a material exposed to a corrosive environment and a constant tensile stress – the corrosion system depicted in Figure 1. Typically, temperature, pressure, solute species, solute concentration, pH, and electrochemical potential are the variables used to describe the environment. Often, specific ions that are present in the environment are the cause of cracking. For instance, carbonate / bicarbonate environments have been shown to produce SCC in carbon steels.⁵ In most cases, the species affecting one system will not have any effect on materials of a different type, e.g., a carbonate / bicarbonate environment may effect carbon steels but may have no SCC effect on aluminum alloys. In addition, the species responsible for SCC is typically not required to be present in large quantities or in high concentrations. Environments causing SCC in specific alloys are well documented and can be used as a design tool to predict whether or not cracking will occur for that particular alloy. However, environments as simple as pure water and dry hydrogen have been known to contribute to SCC.

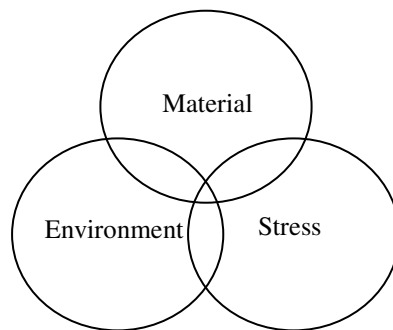


Figure 1. *Illustration depicting a corrosion system.*

Frequently, SCC producing substances are present at levels normally considered harmless, either as components or as impurities in the environment. However, some service conditions can cause locally high concentrations of substances to develop. In the case of a warm buried pipeline, evaporation of ground water allows impurities to concentrate on the pipe surface thereby contributing to SCC. Pre-service conditions are also capable of resulting in SCC failure. For instance, fabrication processes can leave behind residues, shipped or stored pipe may not be protected from a corrosive atmosphere, and piping may be exposed to potentially damaging environments during installation, e.g., welding flux, lubricants, etc.

The conditions for SCC involve service stresses, but often the primary cause can be attributed to manufacturing or installation processes, e.g., welding, thermal processing, surface finishing, and assembly. High levels of residual stresses are capable of being produced by each process. Various other sources resulting in stress concentrations often contribute to mechanical-environmental failures as well. Such sources include accidental third party damage, inclusions, inadequate heat treatment procedures, thermal expansion, and deficiencies in welding.

Research suggests the existence of a threshold stress level. The threshold stress being defined as a stress level below which the probability of SCC occurrence is very low. This stress level depends primarily on the composition of the environment, metallurgical structure of the alloy, and temperature. In the laboratory, it has been shown that cracking may occur at an applied stress as low as 10% of the yield strength; for other metal-environment combinations, the threshold stress is approximately 70% of

yield strength.⁸ Accordingly, there also exists a corresponding threshold stress intensity factor K_{ISCC} . As seen in Figure 2, the crack propagation velocity (V) of SCC systems is often depicted as a function of the applied stress intensity (K_I).⁸

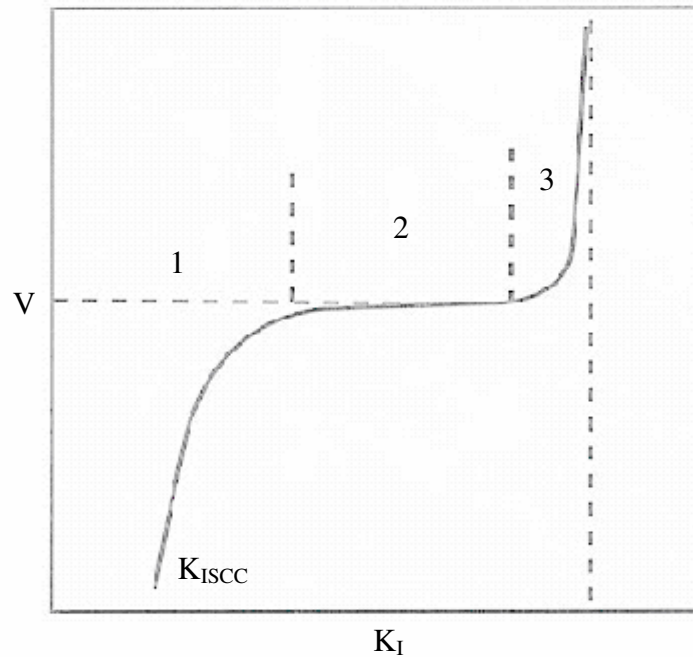


Figure 2. Propagation rate versus the crack tip stress intensity.

The curve in Figure 2 consists of three characteristic stages. In stage 1 the crack growth rate increases rapidly with stress intensity above the threshold, K_{ISCC} . A plateau where the velocity is independent of stress intensity characterizes stage 2. Similar to stage 1, the velocity increases rapidly with increasing K_I in stage 3.

Of particular interest is the regime where the crack propagation velocity is independent of the driving force. This plateau velocity is a function of the particular alloy-environment system and may be greatly affected by alloy composition, heat

treatment, pH, and electrochemical potential. Independence of the driving force indicates that the crack growth rate must be controlled by the rate of a chemical reaction or some other nonmechanical factor.⁸

SCC is capable of occurring in most metals under certain conditions.

Susceptibility of a given metal to SCC in a specific environment depends on its bulk and local chemical composition as well as its metallurgical structure. Significant aspects include phase distribution, grain size and shape, grain boundary precipitation, grain boundary segregation, cold work, and inclusion type and distribution. In general, metals with smaller grain sizes are more resistant to SCC than the same metals having larger grain sizes, regardless of whether or not the cracking is transgranular or intergranular.⁸

Local differences in metal composition, thickness of the passive film, concentration of species, and stress concentration may determine the site of SCC initiation. For instance, thinning of the passive surface layer may result in pitting or grain boundary corrosion. The pit or trench may then act as a stress riser and thus serve as a site for the initiation of SCC. SCC may also be triggered by a preexisting mechanical crack, surface defect, fabrication flaw, or other surface discontinuity.

Electrochemical potential also has a critical effect on stress corrosion cracking, as seen in Figure 3. A passive film is apparently a prerequisite for SCC, but the two zones of susceptibility occur at the potentials where the passive film is less stable. In zone 1, SCC and pitting may occur simultaneously. Pits may result in stress intensification; however, they are not necessarily a prerequisite for the formation of SCC. In zone 2 pitting does not necessarily occur, although SCC may still develop from

the weakness of the passive film at the specific potential range.⁵ Zone 2 SCC is typified by carbon steel in carbonate / bicarbonate solutions.

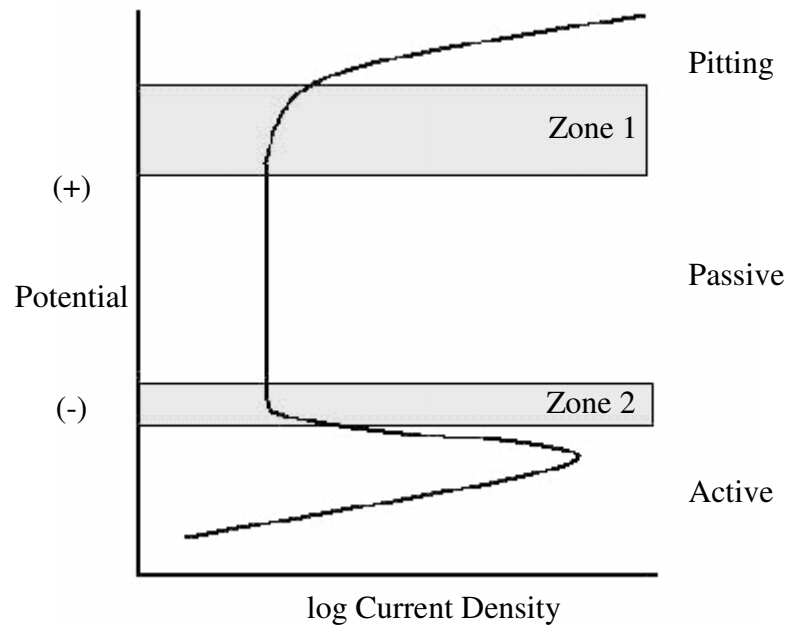


Figure 3. *Potential versus the log of current density.*

Intergranular SCC has been detected on the external surfaces of buried carbon steel linepipe used to transport natural gas. Carbonate and bicarbonate at 75°C (167°F) tends to be the critical environment.⁵ These anions can be found in mill scale, holidays in protective coatings, as well as beneath the coatings in the presence of cathodic protection

Corrosion Fatigue Cracking

Corrosion fatigue cracking (CFC) is the brittle failure of a material caused by a fluctuating stress in a corrosive environment. Accelerated crack initiation and

propagation typically result where neither the environment nor the stress acting alone would be capable of producing a crack. Both alloys and pure metals are susceptible and no specific environment is required. Corrosion products often accumulate during the discontinuous propagation of the crack front.⁵

The frequency of cyclic stress also plays a significant role. Only minor variations in loading are required to accelerate the onset of CFC. Lower frequencies generate larger crack propagation per cycle while very high frequencies may eliminate the effects of the corrosive environment.⁵ Failures originally thought to be purely SCC may actually be the result of a high tensile stress combined with a low amplitude and / or low frequency cyclic stress. For example, some EAC of NGTP's has been traced to vibrations near compressor stations.⁹

Increasing the R value, R being the ratio of minimum to maximum stress, generally decreases corrosion fatigue resistance.⁵ At higher temperatures when creep is possible, R can also have an effect. In noncorrosive environments at ambient temperature the effect of R is much lower and may have no effect on fatigue.⁽¹⁾⁵ In a fatigue loading situation corrosion reduces the stress amplitude, shortens the time to failure, and eventually eliminates the endurance limit.

Notches, surface roughness, and other stress raisers are known to increase susceptibility to corrosion fatigue. Surface damage resulting from pre-exposure to a corrosive environment is also capable of degrading subsequent fatigue life. Often, in

¹ Ambient meaning a room temperature of approximately 24°C (75.2°F) and no applied voltage.

carbon steels, cracks originate at hemispherical corrosion pits serving as stress raisers.⁸ Surface pitting, however, is not necessarily required for CFC of carbon steel.

CFC is similar to SCC in that a brittle fracture occurs in a material that would normally be ductile in the absence of a corrosive environment. Obviously the term fatigue in CFC implies some form of cyclic rather than static stress as typically found in SCC, however, each mode must have at least a partial tensile component. CFC cracks also propagate in a direction perpendicular to the principal tensile stress, as in SCC. Unlike SCC, CFC does not require the presence of a specific corrosion system, i.e., a specific alloy - environment combination. Exposure to any type of corrosive solution will accelerate fatigue failures of both pure metals and alloys. Corrosion products are also more likely to be present in cracks produced by CFC as the cracks typically form more slowly. In the case of SCC, corrosion products are usually absent if the material has not been exposed for a great length of time after crack formation. In contrast to high pH SCC, CFC fractures are often transgranular with a slight amount of branching, similar to fatigue failures.⁵

Hydrogen Induced Cracking

Hydrogen induced cracking (HIC) is defined as a brittle mechanical fracture initiated by the penetration and subsequent diffusion of hydrogen into the crystal structure of a material, particularly highly stressed areas associated with notches. Exposure to hydrogen may occur prior to manufacturing or from hydrogen present in the environment. For example, the reduction of water or acid yield hydrogen in the following reactions:



HIC effects are often reversible prior to the formation of an actual crack. The original properties may be restored through low temperature baking treatments that allow dissolved hydrogen to escape.⁵

Slowly applied static stresses are more likely to allow the hydrogen to diffuse to the potential crack planes. In this regard, HIC has also been referred to as static fatigue, sustained-load cracking, or hydrogen-delayed fracture.

Occurring most often in high-strength steels, HIC can also appear in softer steels that have been heavily cold worked. The hardness, stress level, duration of the sustained load, and the concentration of hydrogen all influence the likelihood of cracking. HIC is most prevalent at lower temperatures and is all but eliminated in steels exposed to temperatures above 200°C (392°F).⁸

HIC typically initiates below the root of a notch. The initiation of HIC may also be advanced by tensile residual stresses. The crack path is often intergranular, however, transgranular morphology may be present.

For a specific alloy there is a stress-intensity value, K_{Ic} , below which HIC does not typically occur. Experimental in nature, this threshold crack tip stress-intensity factor depends on the nominal strength of the unembrittled material, the amount of hydrogen present in the steel, the location of the hydrogen in the microstructure, and the presence of other embrittling elements or microstructural phases.⁸

Similarities to SCC include a brittle fracture occurring in a corrosive environment in the presence of a constant tensile stress. Cathodic polarization, however, is known to enhance HIC but may suppress SCC. HIC cracks are typically unbranched while SCC cracks normally follow a branched pattern. HIC may be produced in a susceptible alloy if hydrogen is liberated on the surface in the presence of a corrosive environment. Alternatively, SCC generation requires a specific alloy-environment combination. The occurrence of HIC in pure metals has been observed more often than that of SCC, however alloys are still generally more susceptible.

STRESS CORROSION CRACKING MECHANISM

A number of mechanisms have been proposed to account for crack propagation of stress corrosion cracks. The primary focus will be on the slip dissolution or film rupture model.

Slip Dissolution / Film Rupture Model

A simple mechanism, the slip dissolution/film rupture model has been successfully applied to predict stress corrosion cracking behavior in a number of alloy-environment systems including pipeline steels in underground environments.¹⁰ The model sets forth two conditions for the subcritical advance of a crack.¹¹ The first criterion being that the sides of the crack must be protected from excessive corrosion. If this criterion is not fulfilled, environmental attack will typically give way to pitting or general corrosion rather than cracking. For this reason, the environments in which this model applies must be passivating, i.e., a protective film is stable inside of the crack. However, this condition may be offset under fatigue conditions when the mechanical crack propagation rate ensures that the total penetration rate exceeds the oxidation rate of the sides.¹¹

The second criterion is the accumulation of strain at the crack tip and the subsequent rupture of the oxide film. Specifically, slip dissolution refers to the emergence of dislocations at the crack tip surface and the resulting rupture of the passive film.¹⁰ Film rupture, on the other hand, refers to the process where strain at the crack tip causes the relatively brittle passive film to rupture. The increase in crack tip strain occurs either because of an increasing stress, or because of constant stress creep

processes. After the film has ruptured, the advance of the crack tip is controlled by oxidation of the fresh surface as illustrated in Figure 4.

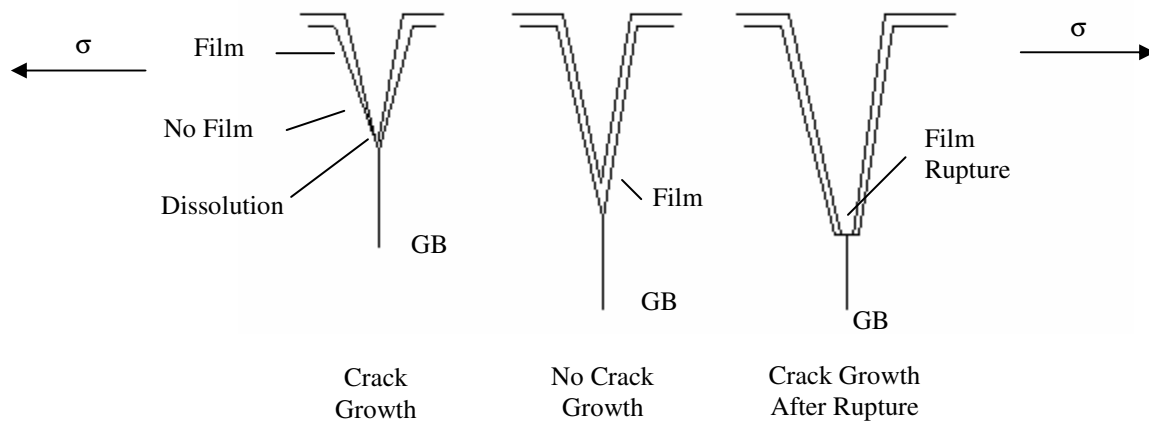


Figure 4. Schematic of an SCC mechanism.

For a given crack tip environment, potential, and material condition, the propagation rate will ultimately be controlled by both the oxidation rate and the frequency of oxide rupture events. Therefore, using Faraday's law and assuming no film rupture, the maximum environmentally controlled crack propagation rate (V_{ctmax}) is related to the anodic current density (i_a) by Equation 3:¹⁰

$$V_{ctmax} = (i_a M)/(z F \rho) \quad (3)$$

where M is the atomic weight of the metal, ρ is the density of the crack tip metal, F is Faraday's constant, and z is the number of electrons involved in the overall oxidation of an atom of metal. For potent cracking environments, crack growth rates of the order of

10^{-6} mm/s are typical for common engineering alloys.¹⁰ The development and rupture of passive films, however, usually result in much lower penetration rates than those predicted by the maximum Faradaic rate. Ford discusses a model that attempts to account for these developments as described in Equation 4:¹¹

$$V_{ct} = (M Q_f \epsilon_{ct}) / (z \rho F \epsilon_f) \quad (4)$$

where Q_f is the oxidation charge per film rupture event, ϵ_{ct} is the crack tip strain rate, and ϵ_f is the fracture strain of the passive film.

The validity of this relationship is limited, however, when crack tip strain rates are either very high or low. At low crack tip strain rates, the tip propagation rate approaches the oxidation rate of the crack sides thereby leading to a blunt geometry and the eventual arrest of the crack. When the crack tip strain rate is high, ductile fracture may outpace dissolution of the bare surface.¹² For ideal SCC conditions, deformation should occur at a faster rate than active area film growth, but not so fast as to outpace the dissolution process. Figure 5 illustrates that above a critical strain rate, film formation cannot keep up with mechanical plastic strain and ductile failure will occur. At strain rates below the critical value, film formation is rapid enough for film ruptures to heal before corrosive events occur again resulting in ductile failure. Figure 5 also illustrates that at low strain rates hydrogen may penetrate into the lattice and reduce ductility.⁵

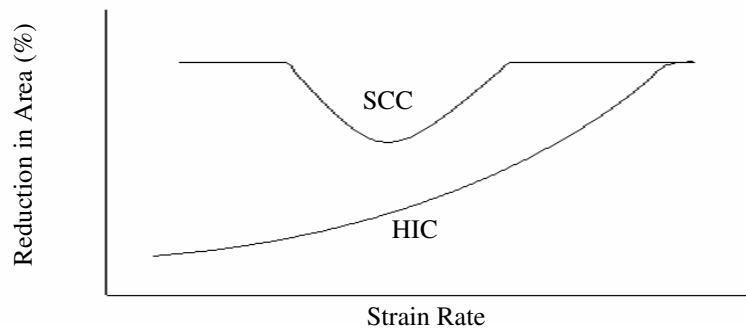


Figure 5. Schematic effect of strain rate on ductility.

As long as K is somewhere between K_{ISCC} and K_{IC} the cracking should be controlled by the slip dissolution/film rupture process. The possible steps that can effect crack propagation by the film-rupture model include: the mechanical properties of the film, the rate of repassivation of the film, the creep rate of the metal at the crack tip, and the kinetics of the corrosion reactions.¹⁰

For constant or increasing load conditions, the SCC propagation rate may be defined by Equation 4. However, when cyclic loading conditions are present the crack is also advancing by cyclic plastic deformation. These two propagation mechanisms, oxidation and fatigue, are considered to occur independently of one another and are therefore additive.¹¹

Stable Oxide Film and Crack Initiation

Several questions arise from the film rupture model, of significant importance is the formation and properties the oxide film. The passive film by definition is a thin surface film developed under oxidizing conditions with high anodic polarization.⁵

Figure 6 indicates that the oxides Fe_2O_3 (hematite or ferric oxide) and Fe_3O_4 (magnetite) are stable over various portions of the Pourbaix diagram for iron.⁵

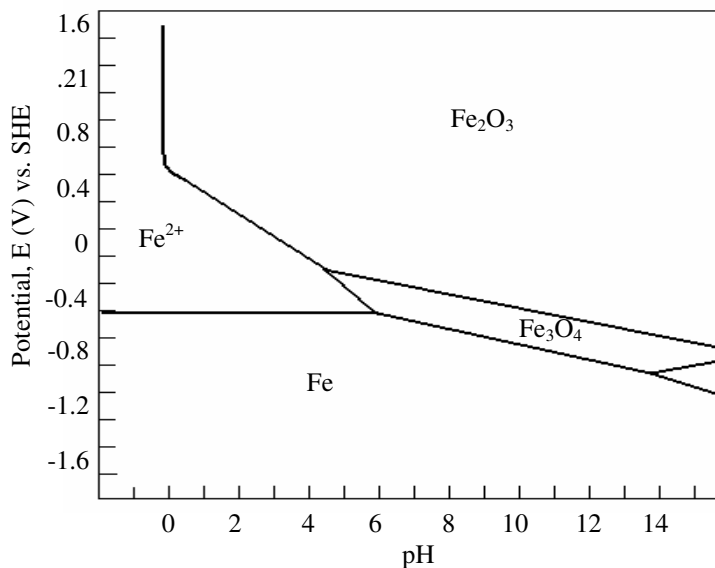


Figure 6. Pourbaix diagram for iron.

The thin, brittle nature of the film impedes its accurate examination, however, thicknesses on the order of 1 to 10 nm and fracture strains of 0.003 have been measured.¹³ In a system consisting of an underground pipeline and its surrounding soil, the oxide films are composed primarily of Fe_3O_4 and FeCO_3 .¹² Their formation is the direct result of electrochemical reactions shown in Figure 7. If the amount of O_2 is limited, then magnetite (Fe_3O_4) can be formed and if carbonate ions (CO_3^{2-}) are present in the groundwater they can combine with the iron ions (Fe^{2+}) to form ferrous carbonate (FeCO_3). These oxide films, in effect, act as barriers to corrosion, thereby reducing the anodic dissolution rate. Ultimately, Figures 6 and 7 illustrate that a chemical reaction

generating a stable oxide film is capable of occurring on the surface of an iron-based pipeline in an underground environment. The stable oxide film is considered one of the necessities for the development of SCC.

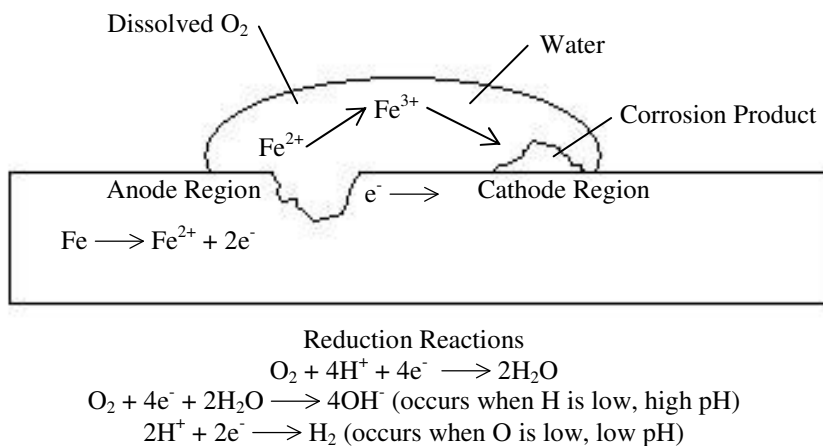


Figure 7. Illustration of the corrosion of iron.

The initiation of SCC may be rooted in local differences in metal composition as well as the thickness of the oxide film. Grain boundary segregation or precipitation can cause the passive layer to be thinned locally allowing a form of grain boundary attack to occur.⁸ It is possible for this corrosion pit as well as pre-existing flaws to act as stress raisers and serve as an initiation site for SCC. Once initiated, the formation of oxide films inside of the crack indicate that a cathodic region is formed along the crack walls and that an anodic region develops at the bare crack tip after the localized strain results in rupture of the film. After rupture of the film the process begins again; the bared metal dissolves and forms another passive layer. The developing crack may become dormant,

coalesce with another crack, or continue to propagate to the point of component failure.

Failure ultimately depends on the specific load, geometry, and material of interest.

PIPELINE MATERIAL

Although pipelines are manufactured from materials conforming to any number of different specifications, the focus of this thesis are those pipes produced under API Specification 5L “Specification for Line Pipe.” The specification covers seamless and welded steel piping that may include plain-end, threaded-end, belled-end, through-the-flow-line, and pipe with ends prepared for special couplings. Ultimately the purpose of the standards is to provide pipe for use in conveying gas, water, and oil in both the oil and natural gas industries.

Specifically, the pipeline material considered is a section of 168.30 mm (6.63 in) diameter, API 5L X52 PSL-2 electric resistance welded pipe with a wall thickness of 7.10 mm (0.28 in) manufactured by the Tex-Tube Company in Houston, Texas. The chemical analysis in wt% is as shown in Table 1:

TABLE 1
Manufacturer’s Chemical Analysis

C	Mn	P	S	Ni	Cr	Cu
0.071	0.700	0.008	0.007	0.011	0.014	0.022
Mo	Si	Al	V	Nb	B	Ca
0.006	0.134	0.028	0.001	0.017	0.0002	0.0030

The complete chemical analysis for the material can be found in Appendix A.

Base material for the pipe is generally steel strip, sheet, or plate in coil form that is either rimmed or killed. Surface condition upon arrival to the pipe mill may be pickled, grit blasted, or as milled. All piping produced at this specific mill is continuous cast steel produced using the basic oxygen or electric arc furnace processes and typically finished to an ASTM grain size between 8 and 9. Ultimately, the transformation of the flat strip into welded pipe is the result of a series of processes including slitting, metal forming, welding, sizing, cutting, finishing, testing, and inspection. Immediately after welding and flash removal, the seam is normalized to a minimum temperature of 871°C (1600°F). In effect, the heat treatment relieves residual stress and softens or removes the martensitic area associated with the heat-affected zone of the weld line thereby providing a controlled microstructure.

API 5L X52 requires that the material's mechanical properties conform to the values shown in Table 2.

TABLE 2

API 5L X52 Mechanical Specifications

Yield Strength , Minimum (MPa / ksi)	Yield Strength, Maximum (MPa / ksi)	Ult. Tensile Strength, Minimum (MPa / ksi)	Ultimate Tensile Strength, Maximum (MPa / ksi)
359 / 52	531 / 77	455 / 66	758 / 110

According to the data supplied by the manufacturer, the yield strength of the pipe sample was 424.7 MPa (61.6 ksi), the ultimate strength was 477.8 (69.3 ksi), the % elongation was 33%, and the Rockwell B hardness was 87.

ENVIRONMENTAL CONSIDERATIONS

For the purposes of this thesis, the environment consists of the external surrounding soil; internal product composition is not considered relevant to the development of external SCC colonies. To a certain extent, the temperature of the pipe's internal product is part of the environment in as much as it effects the temperature of the solution at the pipe to soil interface.

Possibly the most important problem in the avoidance of failures by SCC is predicting the environmental conditions that actually initiate this type of failure. The susceptibility of a material depends not only on the electrolyte composition, temperature, and system potential, but also on the properties of the metal. Therefore, environmental requirements to initiate cracking will vary from alloy to alloy. For example, materials that are more reactive, such as carbon steels, require the environment to be conducive to the development of a passive film, hence the cracking of steels in carbonates. On the other hand, titanium alloys that easily form protective oxide films crack most easily in the presence of halide ions.¹⁴

Carbonate / Bicarbonate

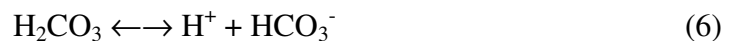
It was once believed that only solutions containing nitrates and hydroxides were capable of producing cracks in ferritic steels. However, nitrate induced SCC has only been observed to occur at potentials more positive than approximately -0.4 V (SCE) while field failures have historically occurred at potentials considerably more negative.¹⁵ Cracking from hydroxide solutions, on the other hand, occurs in a potential range of -0.9 to -1.1 V (SCE) with the necessary concentration of hydroxide ions in the solution

resulting in an electrolyte pH of approximately 14.¹⁵ Concentrations of hydroxides necessary to result in a pH that high typically result in considerable disbonding of the pipeline's protective coating, including: coal tar, asphalt, and polyethylene tapes; however, there is no evidence of such massive disbonding in SCC areas.¹⁵

Research suggested the existence of other ion species capable of producing SCC in buried pipelines. Liquid samples taken between coatings and the pipeline surfaces near SCC failures yielded negligible or near negligible traces of nitrates and hydroxides.¹⁶ The samples were, rather, carbonate / bicarbonate solutions. Crystals of sodium bicarbonate were also found near SCC failures, suggesting that heat transfer from the internal product may be necessary to concentrate the solution and obtain the pH measured at failure, approximately 9 to 10.¹⁶ Subsequent, laboratory tests revealed that concentrated solutions simulating those found in the field near SCC failures were capable of generating SCC in pipeline steels, powerful evidence that the critical environment for SCC is a carbonate / bicarbonate solution.¹⁵

How does this cracking environment develop? There is very little doubt that mild coating deterioration from third party damage will allow the pipe surface to come into contact with groundwater. It is also highly possible that the groundwater will contain some level of carbon dioxide as the result of decaying organic matter in the surrounding soil. For clarification of the relevance of these facts, consider that as the corrosion process proceeds, hydrogen ions will be consumed in the reduction reaction (hydroxyl ions also appear in the solution as the hydrogen ion concentration falls) and the solution pH will increase. Experimentation in simulated groundwater saturated with

carbon dioxide indicates a resistance to this pH increase until a value of approximately 6.5 is reached, at which point the pH will increase sharply until reaching an approximate value of 9.5 and again meeting a resistance. These resistances are attributed to the existence of "side" activities in which the dissolved carbon dioxide is converted to bicarbonate ions at a pH of 6.5 and bicarbonate is converted to carbonate at a pH of approximately 9.5.¹⁵ Equations 5 through 7 illustrate these reactions.



Further experimentation suggests that hydroxide ions can also be produced when cathodic current from a protection system reaches the surface of a pipeline. Ultimately, the pH of the surrounding medium is increased to a value dependent upon the amount of dissolved carbon dioxide. If the amount is too low, then the pH will increase to approximately 11 or 12 and SCC typically will not occur. However, if the dissolved carbon dioxide content is appropriate then the pH will remain around 9.5 and the solution will be buffered by the equilibrium between the carbonate and bicarbonate.¹⁵ At this point, it has been demonstrated that a carbonate / bicarbonate environment with a pH of approximately 9.5 is capable of being generated at the surface of a buried pipeline. In the interest of being thorough, it should also be noted that the temperature of the buried pipeline plays a role in the concentration of the electrolyte. If the water is allowed to evaporate, then the carbonate / bicarbonate solutions can reach saturation resulting in the precipitation of carbonate / bicarbonate crystals. Parkins' research also

suggests that at a given temperature, the potential required for cracking will become less negative as solution pH is decreased and that crack velocity is directly proportional to temperature.¹⁵

The critical potential for SCC has been determined using polarization curves (current density vs. potential) for pipeline steel in carbonate / bicarbonate solutions. Such curves indicate a peak in current density at a potential of approximately -0.65 V (SCE).¹⁵ The peak is followed by current decay suggesting the formation of a film after high levels of anodic activity, both of which are activities necessary to apply the slip dissolution / film rupture model for SCC. Open-circuit potentials for a buried pipeline are typically in the range of or less negative than -0.3 to -0.2 V (SCE).¹⁵ This observation along with other studies by Parkins imply that cathodic protection working in concert with various surface conditions place the pipeline into the appropriate cracking potential.

When the bulk environment is known to promote SCC, the potential for failure is obvious. If the corrosive solution is created by a service-induced reaction such as a high local concentration caused by heat transfer and geometric irregularities, determination of SCC initiation becomes more difficult.

As such, the characteristics of the bulk and local environments become important considerations. If the correct composition is used to simulate the bulk environment then it becomes necessary to determine whether or not it remains constant at the metal-solution interface, as well as the crack tip region.¹⁷

As described previously, gas transmission lines are capable of generating a carbonate / bicarbonate solution at their surface, typically the result of a disbonded coating combined with carbon dioxide dissolved in the soil.¹² However, it is still necessary to consider the possibility of local concentration changes within the cracks themselves. The determination of the occurrence of composition and potential changes within cracks is surrounded with difficulty. If there is a small or restricted volume of liquid then the chemistry of the local solution may change drastically from that of the bulk. In certain instances local acidity may even develop due to a hydrolysis reaction within the crack walls.¹⁴ Additionally, the potential in a crevice may move in and out of the range believed to generate SCC depending on the development of both the internal passive film and hydrogen gas bubbles, the later causing an increase in potential from the cathodically protected value.¹⁵

Complicating matters further, laboratory stress corrosion studies are typically carried out over a period of days, when in reality SCC may develop over a period of months or years. According to research, the pH in a carbon steel crevice is strongly a function of time as well as wet / dry cycling.¹⁸ As such, short-term laboratory tests may not accurately reproduce the long-term nature of the field environment.

EXPERIMENTATION

Theory

The development of a purely mechanistic model requires a complete understanding of the underlying SCC mechanisms as well as its relation to engineering parameters. Although the slip dissolution / film rupture process is generally believed to be responsible for SCC, the actual mechanism is not exactly understood. Therefore, a purely mechanistic approach based on current understanding does not provide a comprehensive foundation for model development. On the other hand, a purely empirical approach requires the availability of an enormous amount of data covering all significant variables; some having complex nonlinear synergistic effects.¹⁹ The lack of comprehensive data, therefore, makes an effective empirical model difficult to develop. As an option, a semi-empirical approach based on currently accepted SCC mechanisms combined with data extracted from experiments might provide useful information for the development of a new growth rate model.

In certain instances, a critical crack depth can be determined from fracture mechanics principles, i.e., through a comparison of the stress intensity factor K_I with the fracture toughness of the material K_{IC} . This critical crack depth could possibly be combined with the time to failure to provide an average rate for crack growth. However, in this study, the crack initiation time cannot be accurately separated from the overall time-to-failure. Complicating matters further, the crack geometry cannot be known prior to initiation; hence K_I must be based on an assumed geometry that may or may not reflect that of the actual crack. Further, SCC typically forms in colonies - clusters of

cracks that initiate, propagate, coalesce, and possibly hibernate at different rates. A model that predicts the behavior of one single crack initiating and developing to the point such that it is capable of causing failure without interaction from adjacent cracks therefore lacks credibility.

Measurable quantities considered in this thesis are time, load, extension, pH, temperature, and potential. The challenge then is to utilize these measurements in the development of a pipeline lifetime prediction model. Considering the uncertainties associated with crack initiation time, geometry, and the effects of coalescence, the development of a "reduction factor" method of characterizing the critical EIC systems is attractive - the critical systems broadly being the environment, the material, and the loading. For instance, an average pipeline lifetime could be adjusted based on factors for material, environment, and load. As an analogy, consider the use of Marin factors when determining the endurance limit of a component subjected to a cyclical load:

$$S_e = k_a k_b k_c k_d k_e S_e' \quad (8)$$

Where S_e is the endurance limit of the part, k_a through k_e are factors that adjust for surface, size, load, temperature, and miscellaneous effects, and S_e' is the endurance limit of the test specimen.

To further elaborate, consider the following equation:

$$L_C = C_1 C_2 \dots C_n L_A \quad (9)$$

Where L_C is the predicted lifetime of the pipeline, C_1 through C_n are specific corrosion mode reduction factors (uniform corrosion, EAC, etc.), and L_A is the lifetime of a test specimen. More specific to the current interests:

$$L_C = C_1 L_A \quad (10)$$

Where C_1 is the reduction factor for EAC and consists of subfactor reflecting the dependency on environment (D_E), load (D_L), and material (D_M), see Equation 11.

$$C_1 = D_M D_E D_L \quad (11)$$

The subfactor may subsequently be broken down to any level at which the effects of various influences are known with some degree of certainty: ultimate strength, surface condition, pH, soil resistivity, temperature, internal pressure, load frequency, etc. Table 3 shows a partial example of the hierarchy.

TABLE 3
Subfactor Hierarchy

C_1		
D_M	D_E	D_L
F_1 - Pipeline Grade (API)	G_1 - Temperature	H_1 - Internal Pressure
F_2 - Age	G_2 - pH	H_2 - Frequency of Loading
F_3 - Surface Condition	G_3 - Potential	H_3 - Intensification Factors
F_4 - Other	G_4 - Other	H_4 - Other

The difficulty arises in the determination of the relationship between each one of these quantities and its associated sub-factor and ultimately the lifetime itself. Clearly it is outside the scope of this thesis to fully explore and develop relationships for all of the pertinent variables. The focus, rather, will be on the data made available through constant extension rate testing (CERT).

For a given extension rate, the time-to-failure for a specimen in a corrosive environment should be less than that of a specimen in ambient conditions. Since all other factors are equal, i.e., the only difference in the two tests is the corrosive environment, the reduced time-to-failure is presumed to be exclusively attributable to the effects of the corrosive environment. The ambient specimen should fail in a predictable ductile manner, while the specimen in the corrosive environment should exhibit a failure that is considerably more brittle if EAC is, in fact, present.

Experimental Description

The overall experiment consists of 6 constant extension rate tests of the X52 pipeline steel; 3 in ambient conditions and 3 in conditions simulating the external surface of an underground pipeline. The ambient tests are intended to generate a baseline for the comparison of the behavior observed in the corrosion tests. Each of the three ambient tests will be performed at a unique extension rate ranging from 2.54×10^{-4} mm/s to 5.08×10^{-5} mm/s (1×10^{-5} in/s to 2×10^{-6} in/s) in accordance with the recommendations provided in ASTM Standard G 129. The corrosion tests will then be performed at the same extension rates as their ambient counterparts. Ultimately, data extracted from the corrosion tests will be compared to the baseline data to examine the effects of the corrosive environment.

Due to the complex nature of varying soil compositions, specific soil samples are not included in this analysis. Rather, the environment is reproduced using a groundwater simulation solution replicating environmental parameters known to produce cracking conditions: 0.11 g/L of potassium chloride, 0.49 g/L of sodium bicarbonate, 0.18 g/L of

hydrated calcium chloride, and 0.13 g/L of hydrated magnesium sulfate.²⁰ Test conditions consisted of a temperature of 75°C (167°F), pH of approximately 9, and a potential of -0.65 V SCE.¹⁵

Equipment and Setup

The experimental setup for both environments consisted of a Cortest constant extension rate test machine controlled by a Cortest SC 12 controller. Time, load, and crosshead extension data were acquired using a Soltec 1243 strip chart recorder. The pipeline simulation tests included the addition of a Cortest 316 stainless steel and glass environmental chamber, Cortest model HT-10 temperature controller, an Orion model SA520 pH meter, and an AIS Model PEC-1 potentiostat with a graphite counter electrode, and a Fisher Scientific 13-620-258 saturated calomel electrode (SCE) for reference. See Figure 8 for an illustration of the experimental setup.

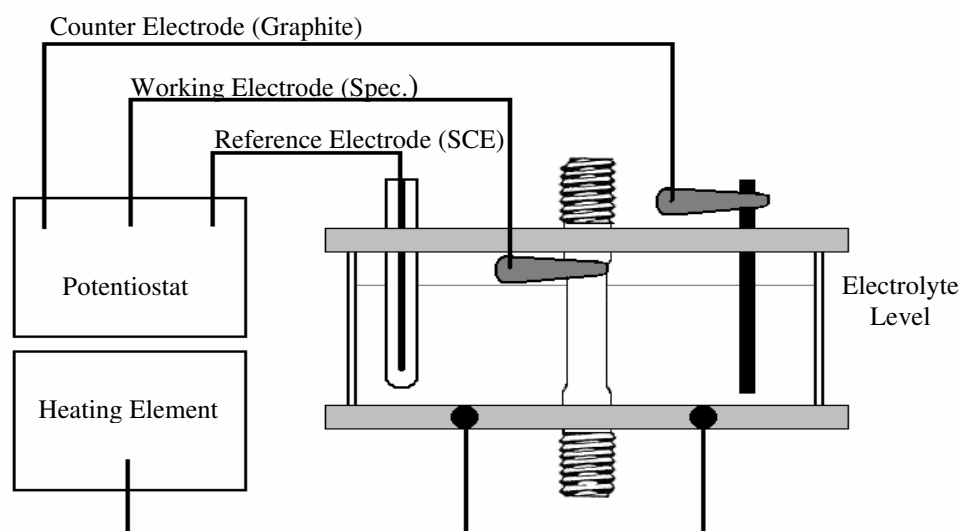


Figure 8. Schematic of the experimental setup.

The control scheme for the CERT was such that the jack screw motor drive rpm was the only operator input. As such, it was necessary to determine the relationship between motor rpm and crosshead extension rate (calibration data can be found in appendix B). Ultimately, the goal was to achieve the same crosshead extension rate for tests 1 and 4, 2 and 5, and 3 and 6.

Test Specimens

As shown in Figure 9 the test specimens were machined to dimensions that would not exceed the capacity of the CERT machine.

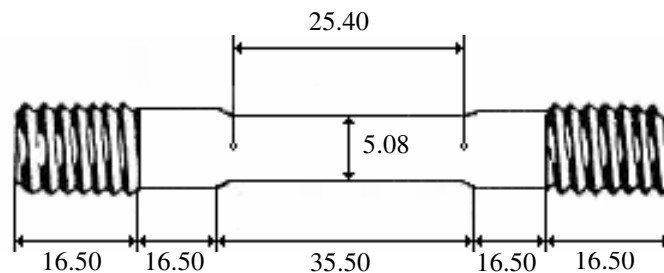


Figure 9. *Diagram of the CERT specimen.*

All dimensions are in mm.

Since the major thread diameter of the specimen is limited by the wall thickness of the available pipe section, the geometry does not conform to any known standard. The unique nature of the specimen also required the machining of two new adapters to allow installation into the CERT machine. In order to conduct CERT's on this material the pipe sections were machined into specimens with geometry appropriate for use in the

Cortest load frame. The specimens were cut from longitudinal sections of the pipe wall - the available pipe diameter and thickness were much too small to allow specimens to be cut from lateral sections. The sections were then turned on a lathe to achieve the desired dimensions. In both the ambient and corrosion tests the specimens were installed as-machined, i.e., they were not polished or ground, the as-machined dimensions are listed in Table 4. A 25.4 mm (1.0 in) gauge length was marked on each specimen and ultimately used to determine the % elongation.

TABLE 4

Initial Dimensions of the Test Specimens

Specimen	Initial Gauge Length (mm/in)	Initial Gauge Diameter (mm/in)	Initial Area (mm ² /in ²)
1	25.40 / 1.00	5.08 / 0.20	20.27 / 0.03
2	25.04 / 0.99	5.08 / 0.20	20.27 / 0.03
3	25.17 / 0.99	5.08 / 0.20	20.27 / 0.03
4	25.17 / 0.99	5.05 / 0.20	20.03 / 0.03
5	25.17 / 0.99	5.08 / 0.20	20.27 / 0.03
6	26.09 / 0.99	5.08 / 0.20	20.27 / 0.03

EXPERIMENTAL RESULTS AND DISCUSSION

CERT Test Results

At the conclusion of each test, the overall extension of the crosshead and the test duration were used to determine the average extension rate as shown in Table 5. From the difference in the fracture stresses shown in Table 6 it appears that the corrosive environment did have an effect on some of the mechanical behaviors of the specimens. Of particular note were the differences in reduction of area between samples 1 and 4 and 3 and 6. This drop in the reduction of cross sectional area is indicative of a loss in ductility - an observation associated with EAC. Curiously, the drop in reduction of area between specimens 2 and 5 was much less pronounced.

TABLE 5
CERT Data

Test	Duration (hr)	Extension Rate (mm/s)	Final Gauge Length (mm / in)	Final Gauge Diameter (mm / in)	Final Area (mm ² / in ²)
1 Ambient	12.10	0.23x10 ⁻⁰³ / 9.20x10 ⁻⁰⁶	34.49 / 1.36	2.57 / 0.10	5.17 / 0.01
2 Ambient	16.58	0.11x10 ⁻⁰³ / 4.40x10 ⁻⁰⁶	31.06 / 1.22	2.59 / 0.10	5.27 / 0.01
3 Ambient	42.48	0.06x10 ⁻⁰³ / 2.20x10 ⁻⁰⁶	31.14 / 1.23	2.62 / 0.10	5.38 / 0.01
4 Corrosive	8.20	0.22x10 ⁻⁰³ / 8.80x10 ⁻⁰⁶	30.81 / 1.21	2.95 / 0.12	6.82 / 0.01
5 Corrosive	17.38	0.11x10 ⁻⁰³ / 4.40x10 ⁻⁰⁶	30.63 / 1.21	2.69 / 0.11	5.69 / 0.01
6 Corrosive	36.05	0.06x10 ⁻⁰³ / 2.20x10 ⁻⁰⁶	32.46 / 1.28	3.05 / 0.12	7.30 / 0.01

TABLE 6
CERT Mechanical Results

Test	Load, Ult. (N/lb)	Load, Frac. (N/lb)	Ultimate Stress (MPa/ksi)	Fracture Stress (MPa/ksi)	% Reduction in Area	% Elongation	Total Extension (mm/in)
1	9998 / 2248	5553 / 1248	493 / 72	1074 / 156	74.50	35.80	10.15 / 0.40
2	9678 / 2176	5522 / 1241	478 / 69	1048 / 152	73.99	24.04	6.73 / 0.26
3	9802 / 2204	5513 / 1239	484 / 70	1026 / 149	73.48	23.71	8.58 / 0.33
4	9691 / 2179	5469 / 1229	483 / 70	802 / 116	66.02	22.40	6.60 / 0.26
5	9295 / 2090	5006 / 1125	459 / 67	879 / 127	71.91	21.70	6.92 / 0.27
6	9158 / 2059	5246 / 1179	452 / 66	719 / 104	64.00	24.44	7.26 / 0.29

The durations for tests 1 through 3 were as expected, with test 1 having the shortest and test 3 the longest. Tests 4 through 6 indicated a similar pattern. The key observation, however, lies in the fact that test 4 terminated 32% sooner than test 1. Similarly, test 6 reached failure 15% sooner than test three. Both observations suggest that the environment was indeed having an effect on the test specimens. Again, tests 2 and 5 differ from the norm; test 5 actually took 5% longer to fail than test 2. As a whole, the values in Table 6, excluding % elongation for test 6, were lower for the corrosive tests than the ambient tests. In some cases the differences are minor, e.g., the differences in ultimate load between tests 1 and 4. Lowered values of ultimate stress for the corrosive tests were a direct result of the small differences in ultimate load. The differences in fracture loads themselves were small, but when divided by the final area of the corrosive test specimens the differences resulted in appreciable distinction

between fracture stresses of the ambient and corrosive tests. Ultimately, fracture stress and % reduction in area appear to have been affected most by the environment.

An examination of Figure 10 suggests that the specimens tested in the corrosive environment had a lower modulus of toughness, however the general shapes of the curves are still those of a ductile material.

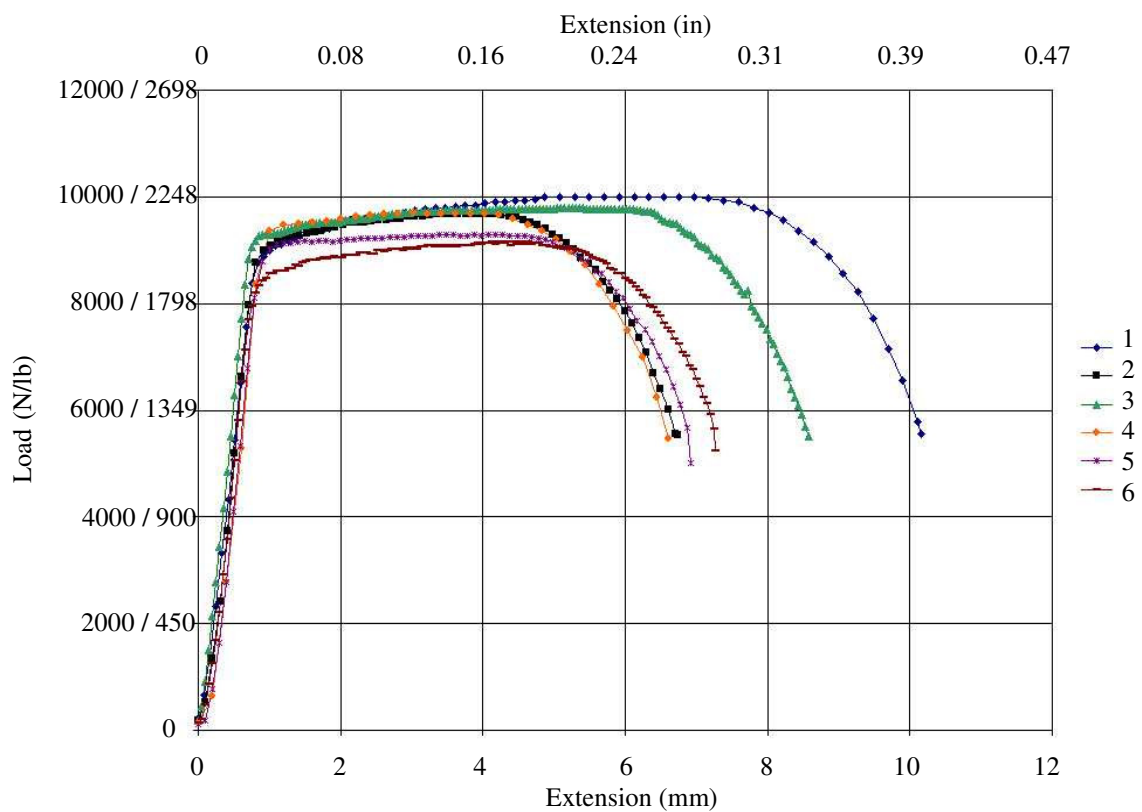


Figure 10. Load / extension curves for each specimen.

Table 7 indicates the % differences for the CERT data determined in the ambient tests and the corresponding corrosive tests. Each of these differences was determined by

dividing the difference between the ambient and corrosive test value by the value for the ambient test and multiplying by 100. Positive values indicate that the ambient test had a greater magnitude. The larger percent differences between fracture stresses tend to indicate that the corrosive environment in this study most directly affected this behavior.

TABLE 7
% Changes in CERT Data

Test	Ultimate Load	Fracture Load	Ultimate Stress	Fracture Stress	% Reduction in Area	% Elongation	Time to Failure
1 & 4	3.07%	1.52%	2.09%	25.34%	11.38%	37.43%	32.23%
2 & 5	3.95%	9.34%	3.95%	16.05%	2.81%	9.74%	-4.83%
3 & 6	6.58%	4.84%	6.58%	29.89%	12.90%	-3.06%	15.13%

Since the elongation of the specimen does not occur uniformly through the gauge length, percent elongation is not typically a quality indicator for a loss of ductility. There is, however, still an observation to be made. In general, results indicated that the differences in percent elongation between ambient specimens and specimens in the groundwater simulation solution increased with increasing extension rate, suggesting further that the environment was affecting the behavior of the specimens. Figures 11 through 13 graphically summarize the remaining information from Tables 3 and 4.

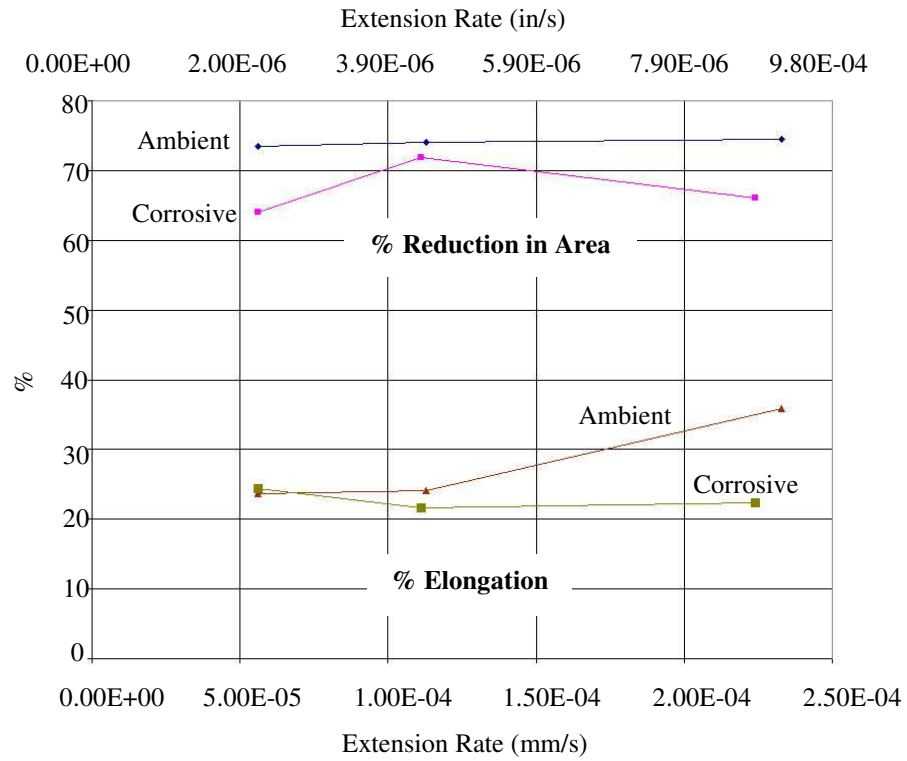


Figure 11. Graph depicting % elongation and % reduction in area.

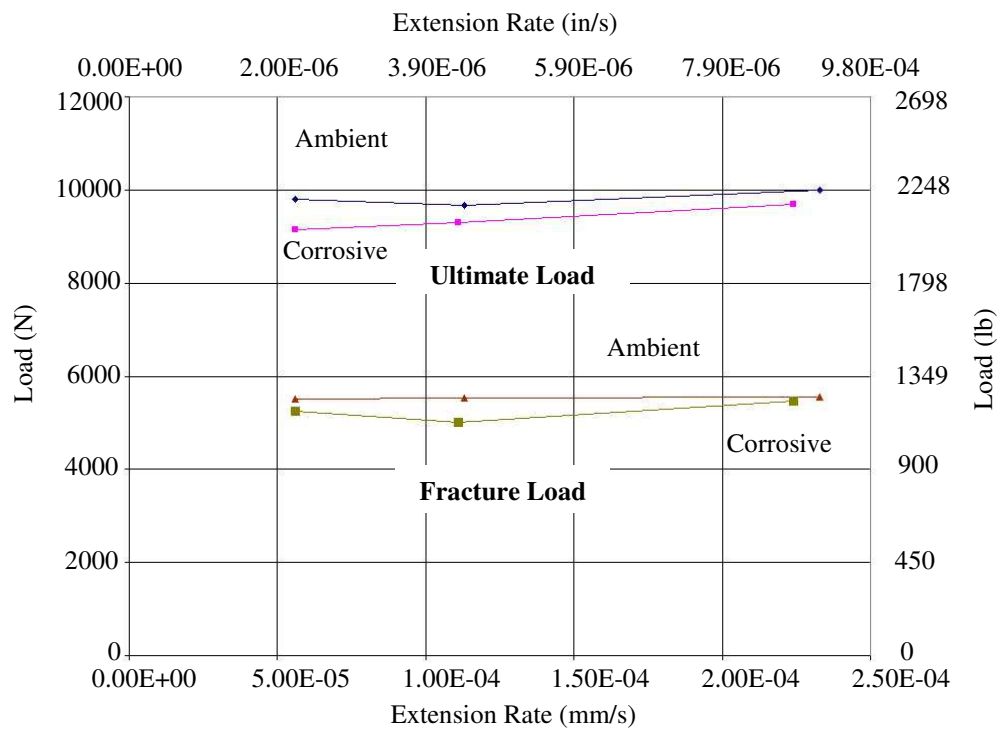


Figure 12. Graph depicting fracture and ultimate loads.

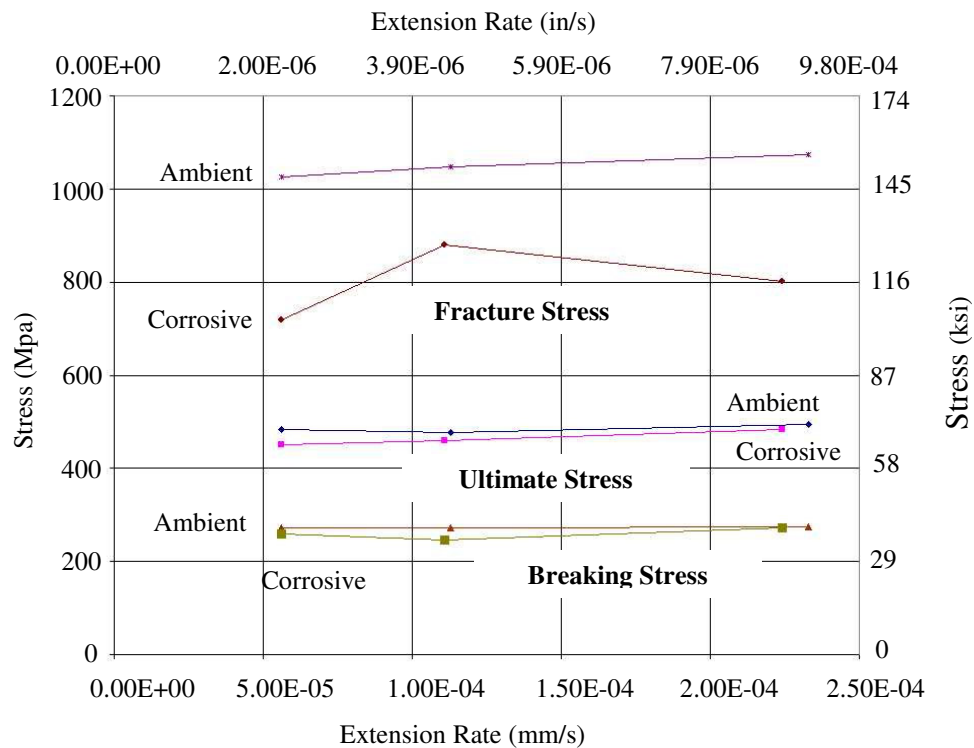
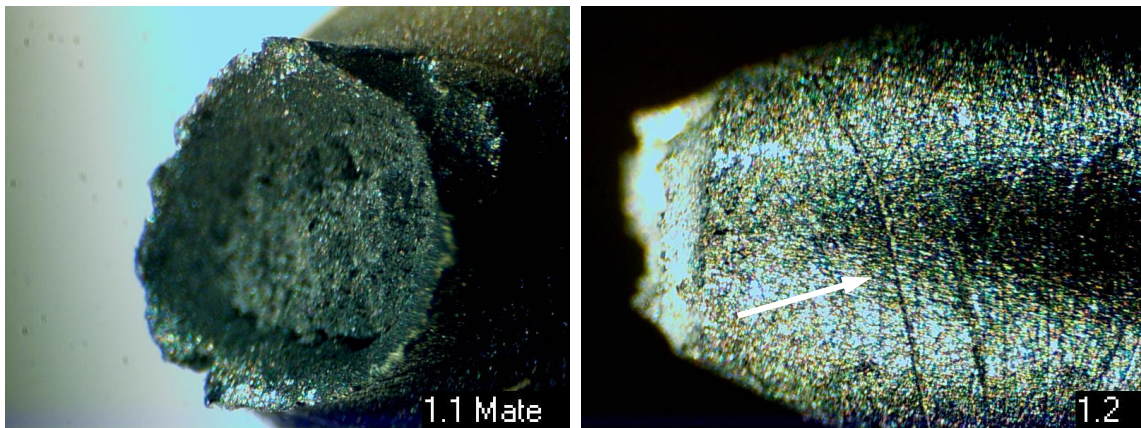


Figure 13. Graph depicting the fracture, ultimate, and breaking stresses.

Visual Inspection

Images from the stereomicroscopic inspection of specimen 1 illustrate fracture of the material along the planes of maximum shear stress; the so-called "cup and cone" failure common for a ductile material as shown in Figure 14(a). The specimen exhibits no visible form of corrosion or cracking, however, tool marks from the machining processes are readily apparent in Figure 14(b). Note that the specimen dimensions exceeded the depth of field for this particular device, as such, only portions of the specimen appear in focus.

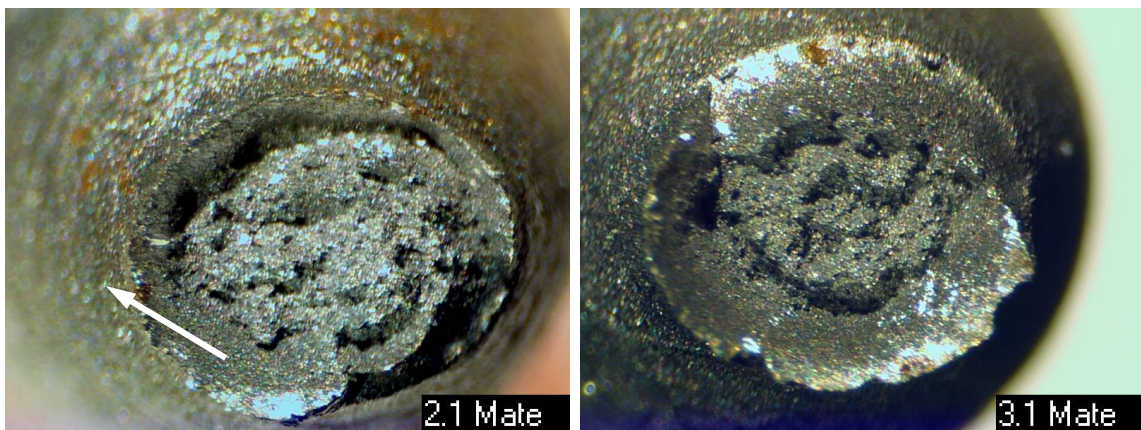


(a)

(b)

Figure 14. Visual inspection of test specimen 1.

(a) Fracture surface of specimen and (b) tool marks visible on specimen 1 (arrow).



(a)

(b)

Figure 15. Visual inspection of test specimens 2 and 3.

(a) Specimen 2 fracture surface with corrosion (arrow) and (b) specimen 3 fracture surface.

Portions of specimens 2 and 3 are depicted in Figure 15. Similar to specimen 1, the "dull" appearance of a typical ductile fracture is clearly visible. Small portions of reddish, brown corrosion product are discernible on both specimens. These particular areas of corrosion developed after testing as a result of exposure to the atmosphere. As was the case with specimen 1, no cracking was apparent on either specimen 2 or 3.

Specimen 4, the first to be tested in the corrosive environment, exhibited regions strikingly different from those of the previous three tests. Each of the fragments from test 4 was covered with reddish-brown and black surface corrosion, an observation consistent with the formation of hematite and magnetite films. Of significant interest is the fracture surface on one of the components. Figure 16 reveals a fracture surface with a ductile central area surrounded in part by a smooth, shiny plateau - the smooth, shiny features being typically indicative of cleavage fractures.

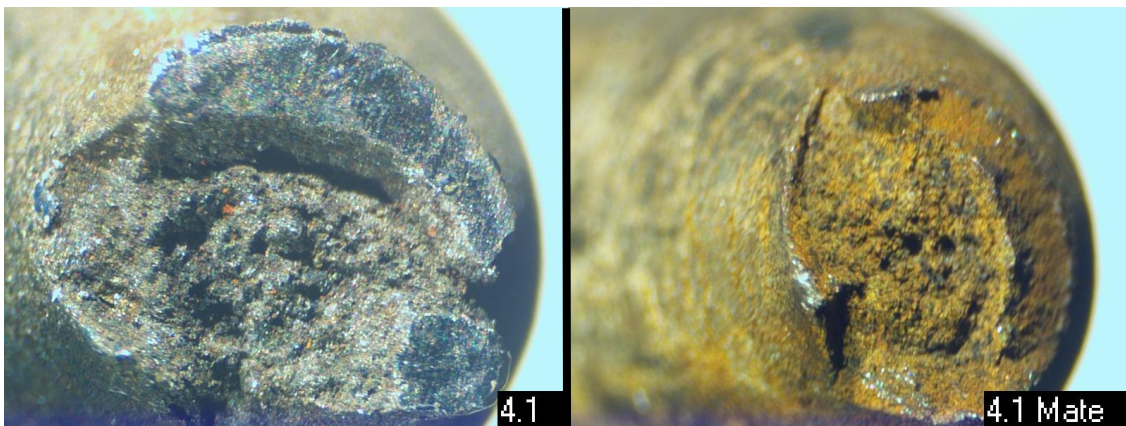


Figure 16. *Visual inspection of test specimen 4.*

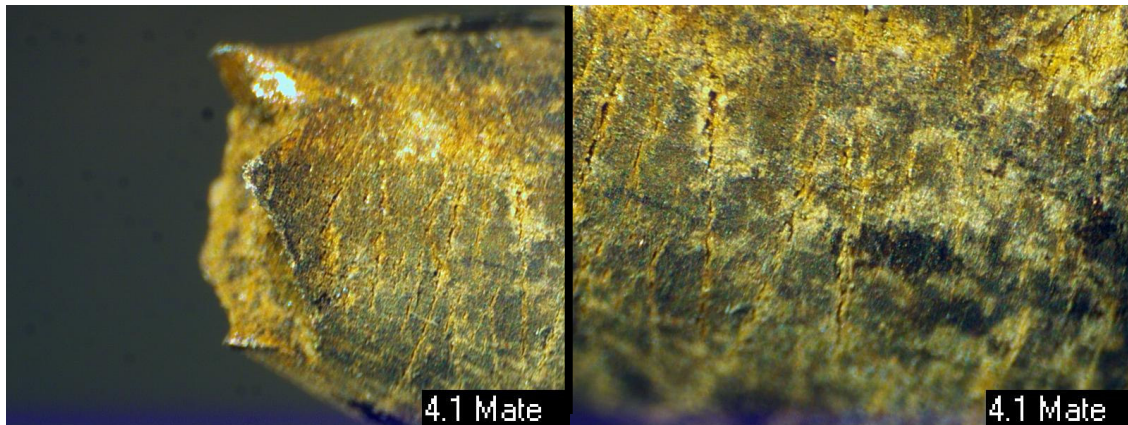


Figure 17. Visible “cracks” on test specimen 4.

Specimen 4 also developed cracks aligned in directions generally perpendicular to the applied tensile load as shown in Figure 17. The orientation of the cracks also suggested that the pre-existing tool marks could have served as initiation sites.

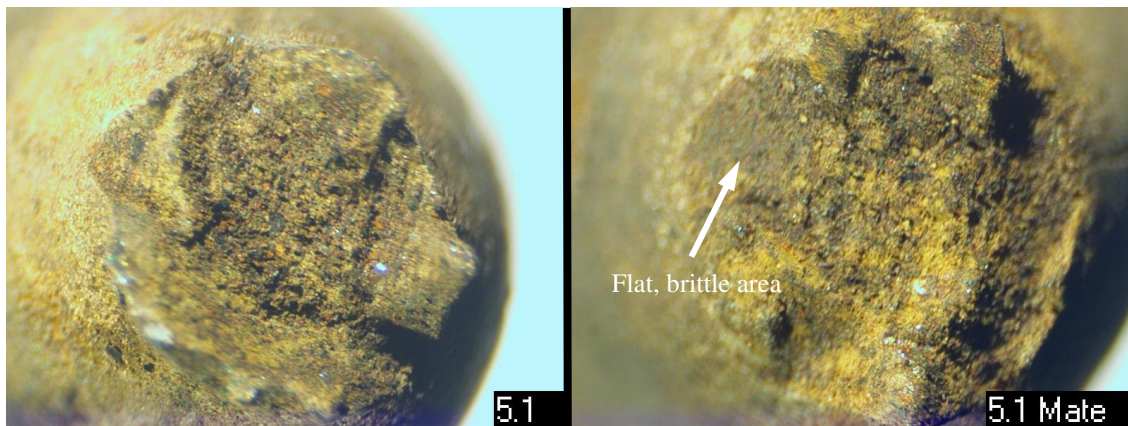


Figure 18. Visual inspection of test specimen 5 – fracture surfaces.

Specimen 5 developed the same reddish-brown and black coating as specimen 4. Although the extension rate for test 5 was between that of tests 4 and 6, both of which

had surface cracks, specimen 5 had no indication of any cracking even though the presence of tool marks was observed. The fracture surface also appeared to have areas where failure was of a brittle nature, as shown in Figures 18 and 19.

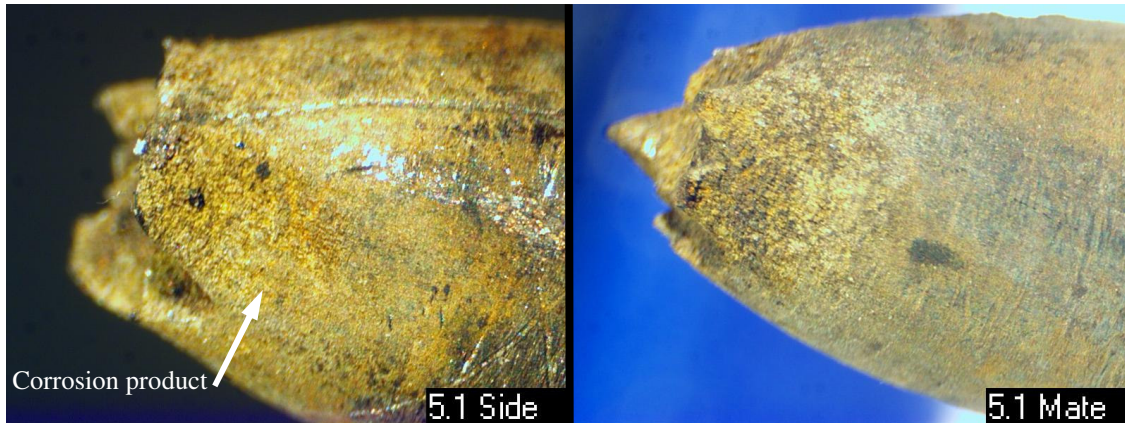


Figure 19. *Visual inspection of test specimen 5 – side views.*

Specimen 6 formed a reddish-brown and black surface coating, partially visible in Figure 20, similar to specimens 4 and 5. Figure 21 also indicates the presence of surface cracks similar in geometry to those of specimen 4. The specimen 6 fracture surfaces contained the same jagged edge topography as found in specimens 4 and 5. Rather than having the traditional cup-and-cone appearance, it looked as though the circumferential fracture lines followed the pre-existing tool marks or the cracks that may have initiated at those locations.

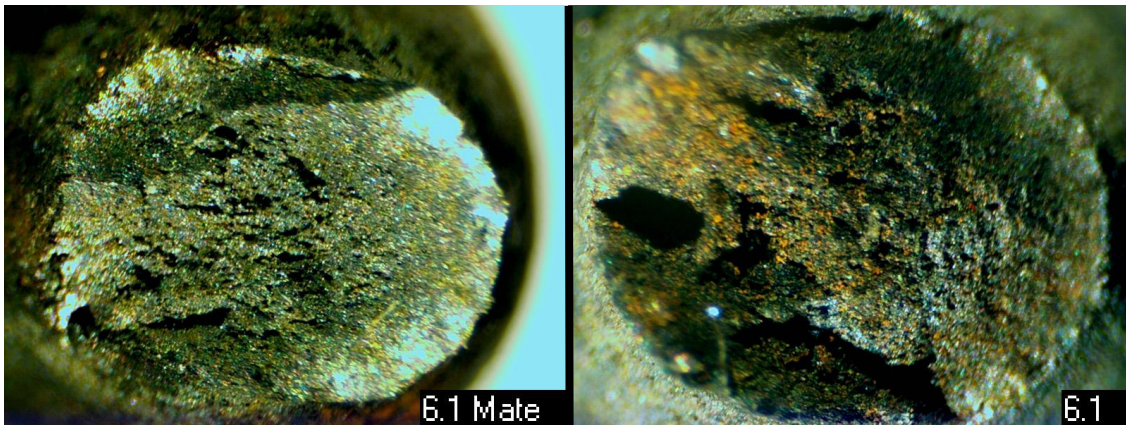


Figure 20. *Visual inspection of test specimen 6 – fracture surfaces.*

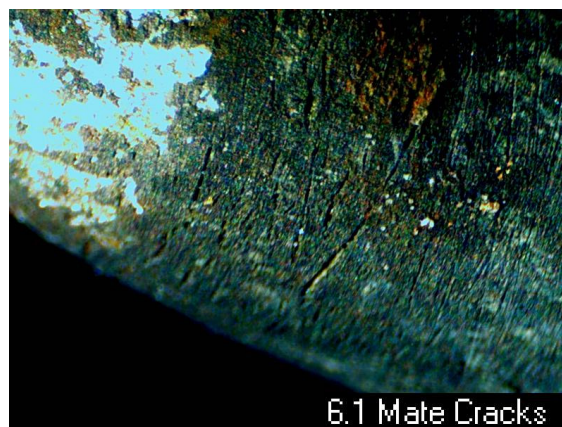


Figure 21. *Visual inspection of test specimen 6 – side view.*

Typically if SCC is present, areas of darkened corrosion product will be visible on the fracture surfaces. No such areas were observed on any specimen evaluated in this study.

Scanning Electron Microscopy

After stereomicroscopy, the samples were analyzed utilizing an environmental scanning electron microscope (SEM). Figures 22 through 24 present side-by-side images of central portions of the fracture surfaces for each set of tests: 1 and 4, 2 and 5, and 3 and 6. Each image is at 400x and all micron markers represent 50 μm .

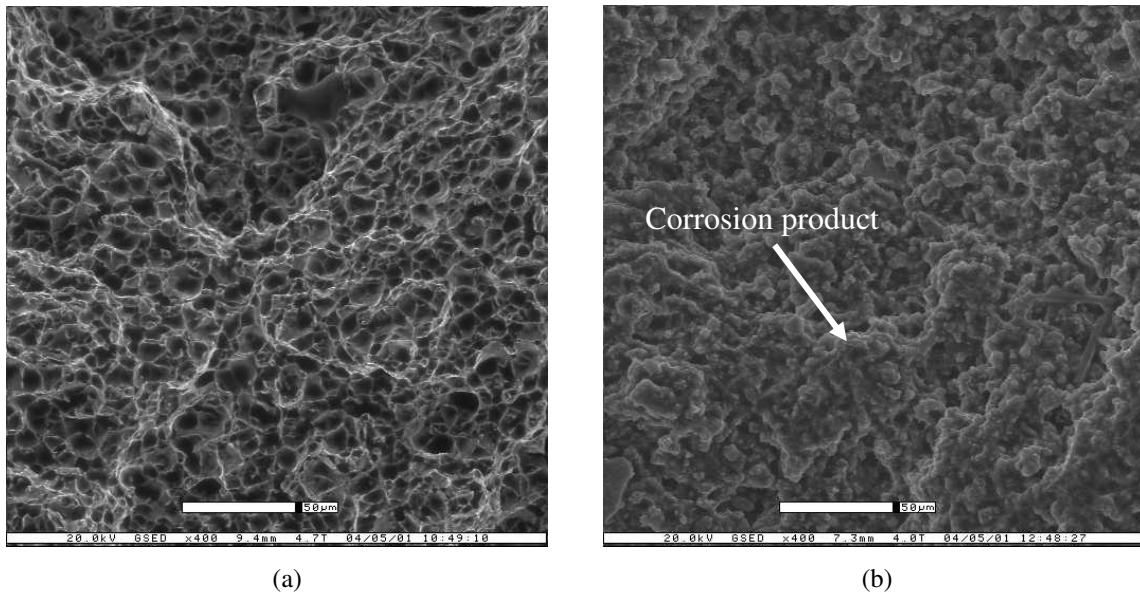


Figure 22. SEM images of test specimens 1 and 4.

(a) Test specimen 1 with no corrosion and (b) test specimen 4 with corrosion product.

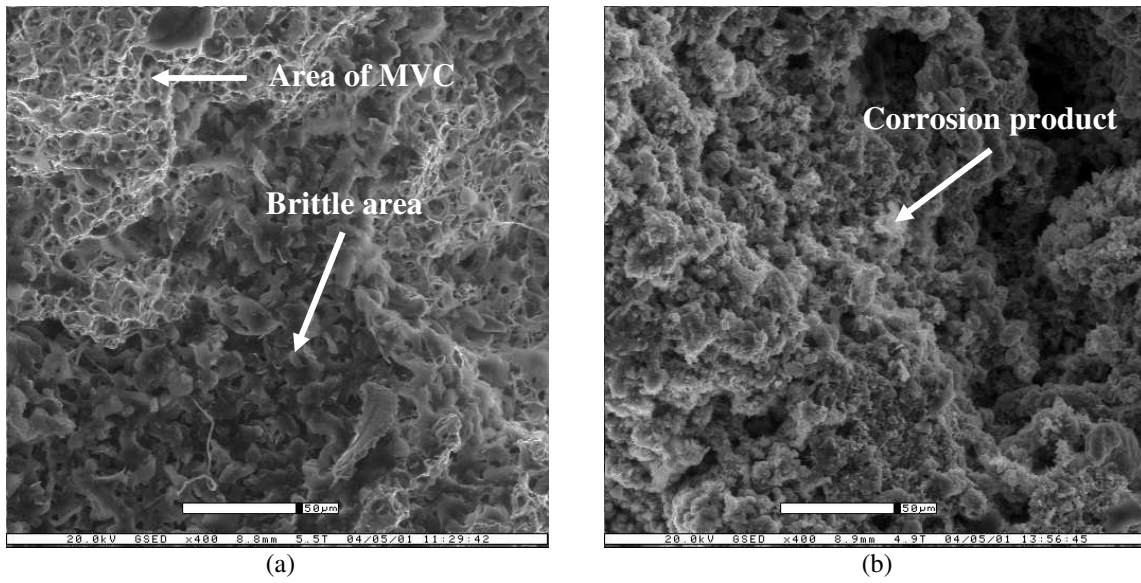


Figure 23. SEM images of test specimens 2 and 5.
 (a) Specimen 2 and (b) specimen 5.

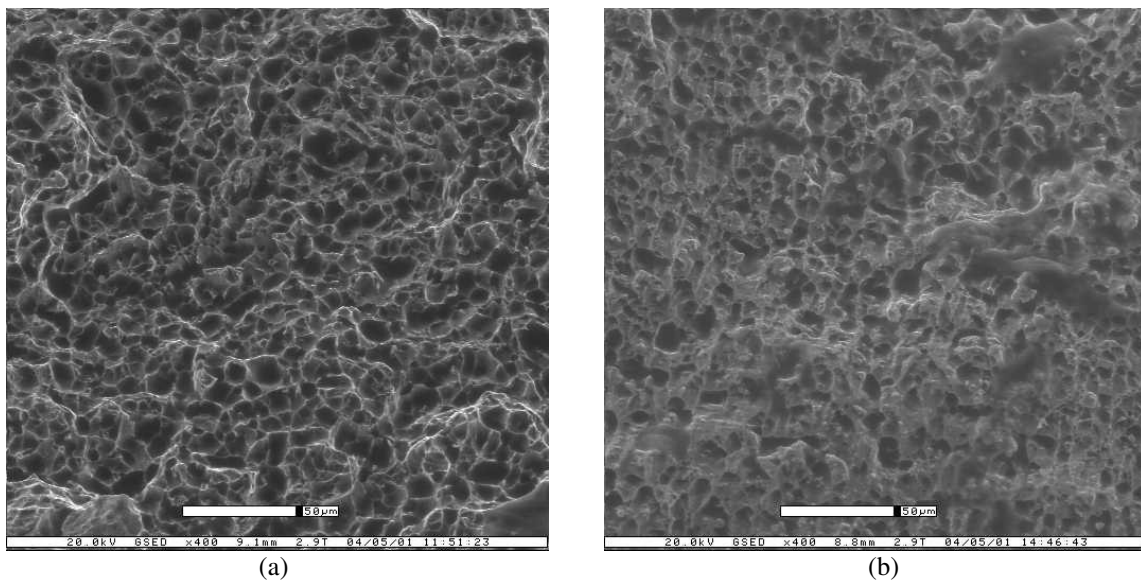


Figure 24. SEM images of test specimens 3 and 6.
 (a) Specimen 3 and (b) specimen 6.

It is readily apparent from the dimples in Figures 22(a) and 24(a) that micro-void coalescence (MVC) occurred and that the failures in these areas were of a ductile nature. As shown in Figure 23(a), specimen 2 appeared to have areas of MVC and small portions of areas that failed in a brittle manner. The images of specimens 4 and 5, Figures 22(b) and 23(b), indicate a small amount of corrosion product on the fracture surfaces. Specimen 6 had little corrosion, if any at all. Figure 25 shows the fracture surface of specimen 5 after ultrasonic cleaning in demineralized water, the presence of MVC is still pronounced indicating that failure was still primarily ductile.

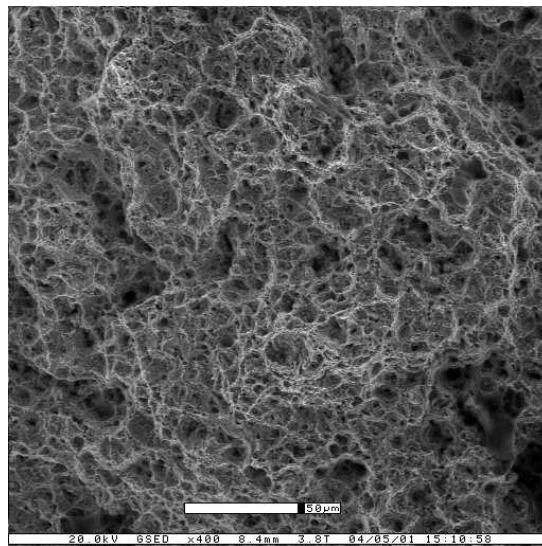


Figure 25. SEM image of test specimen 5 after cleaning.

Figures 26 through 28 are images of the apex of the free surface and the inside surface of the shear lip for each of the specimens. The voids in this area are somewhat parabolic in shape, indicative of the presence of shear. Corrosion product is visible filling in the dimples on all of the specimens tested in the corrosive environment.

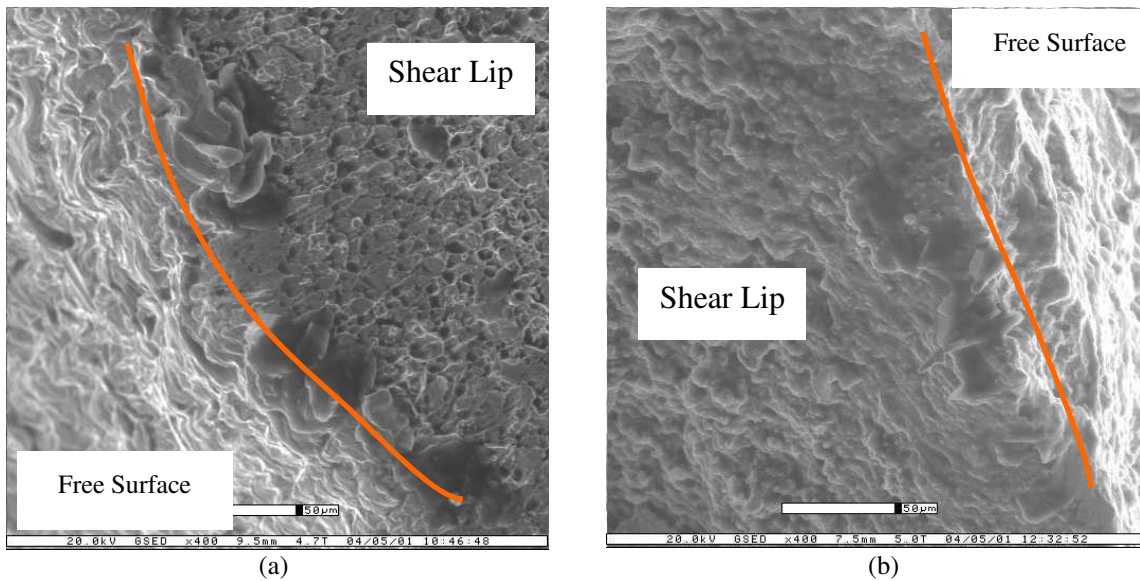


Figure 26. SEM images of test specimens 1 and 4 – shear lip.
(a) Specimen 1 and (b) specimen 4.

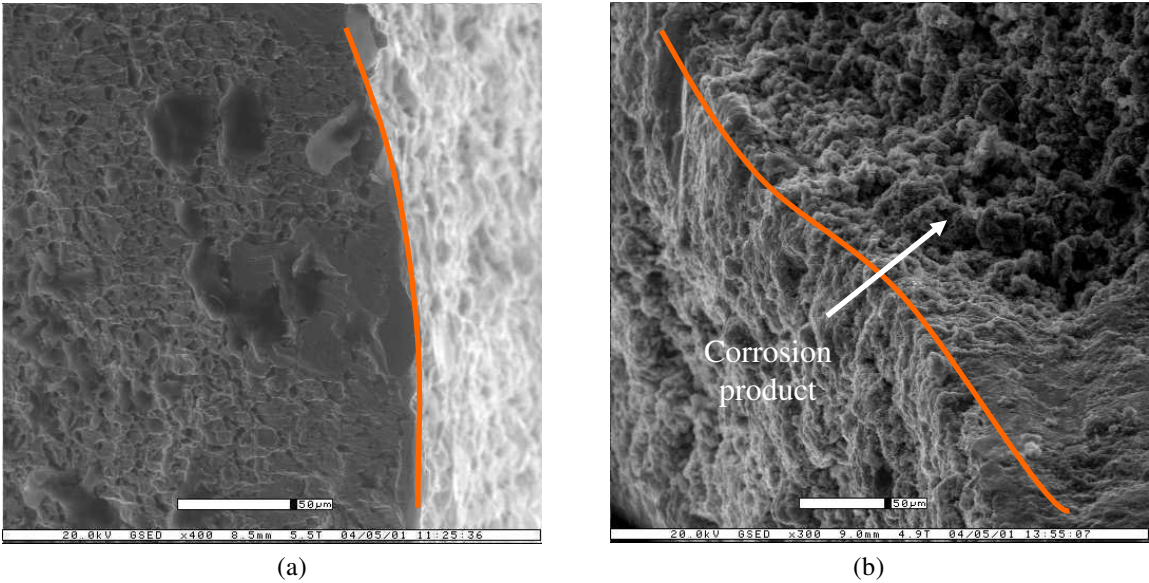


Figure 27. SEM images of test specimens 2 and 5 – shear lip.
(a) Specimen 2 and (b) specimen 5.

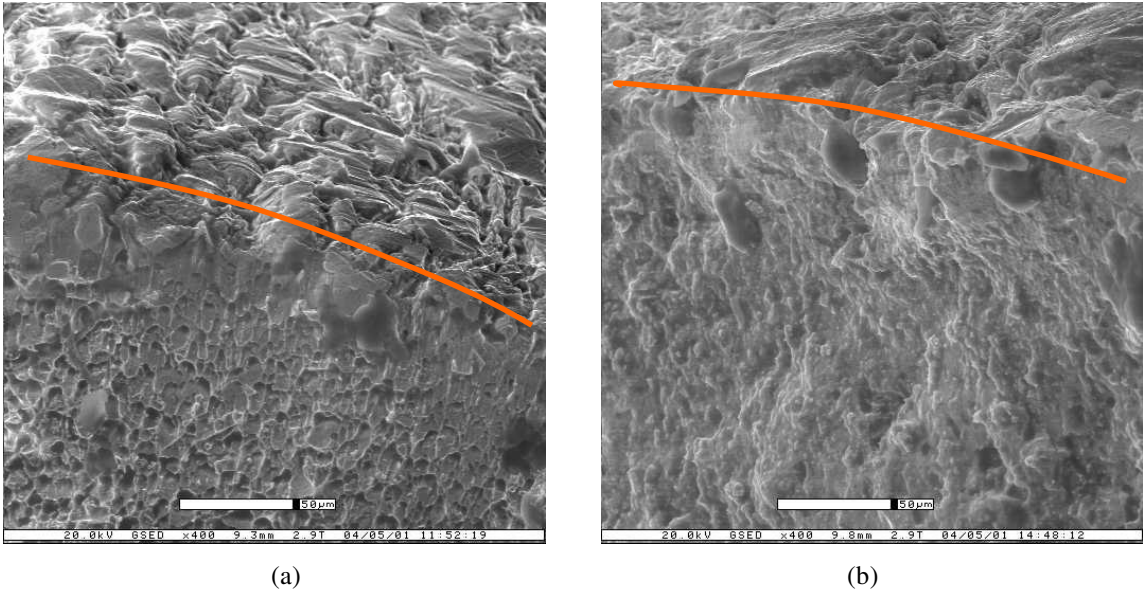


Figure 28. SEM images of test specimens 3 and 6 – shear lip.
(a) Specimen 3 and (b) specimen 6.

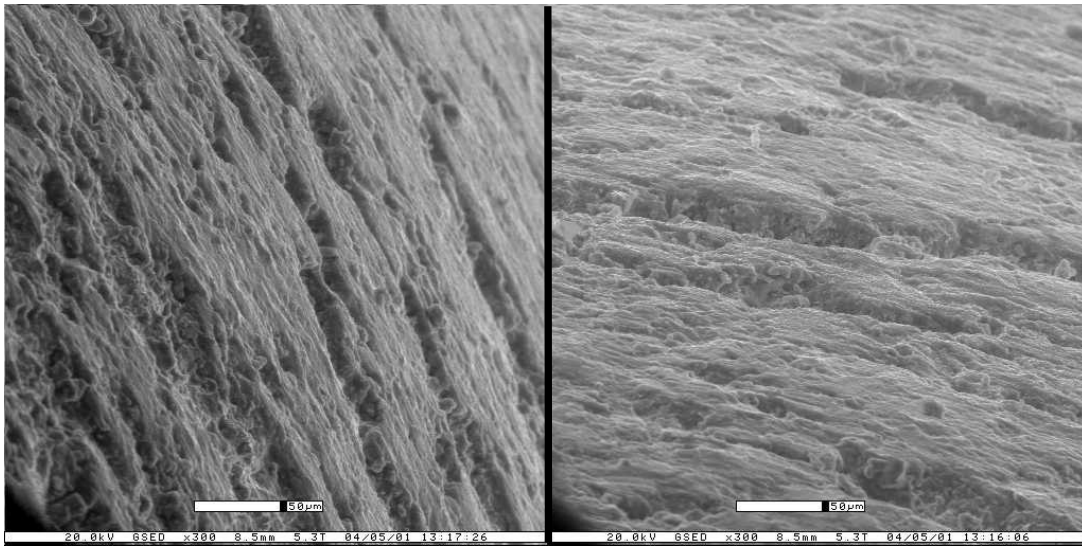


Figure 29. SEM images of test specimen 4.

Figure 29 depicts images of the free surface near the plane of fracture of specimen 4. The images reveal the presence of crack-like formations around the entire circumference of the specimen. It is unclear whether or not the formations penetrate into the substrate material and whether they are the result of tool marks or the environment.

Further investigation of the fracture surface of specimen 4 uncovered the presence of smooth areas lacking MVC, indicative of brittle fractures, as shown in Figures 30 and 31. These surfaces do not have the typical “rock-candy” appearance of intergranular fracture and appear to be transgranular in nature.

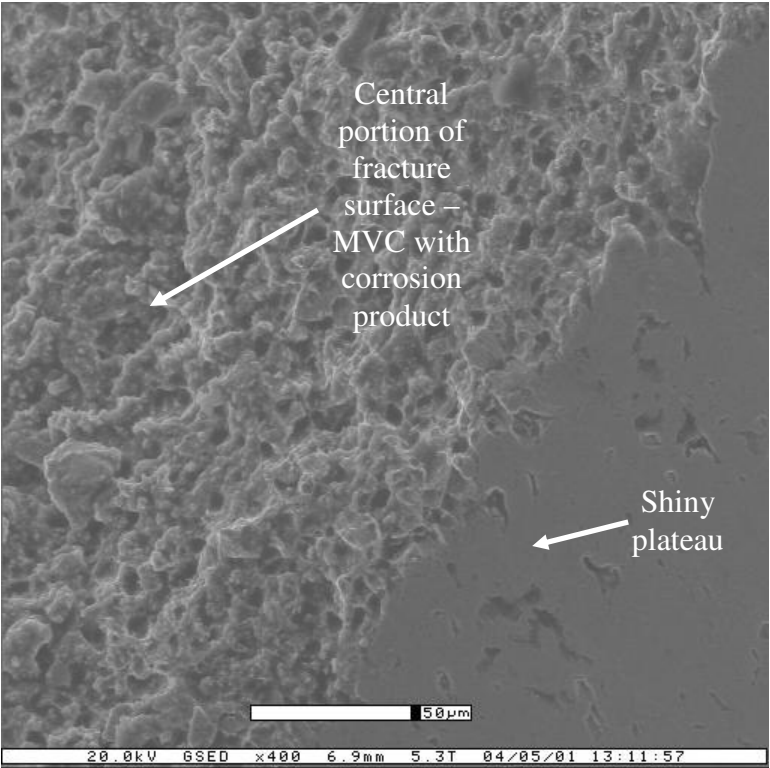


Figure 30. SEM image of the fracture surface of test specimen 4.

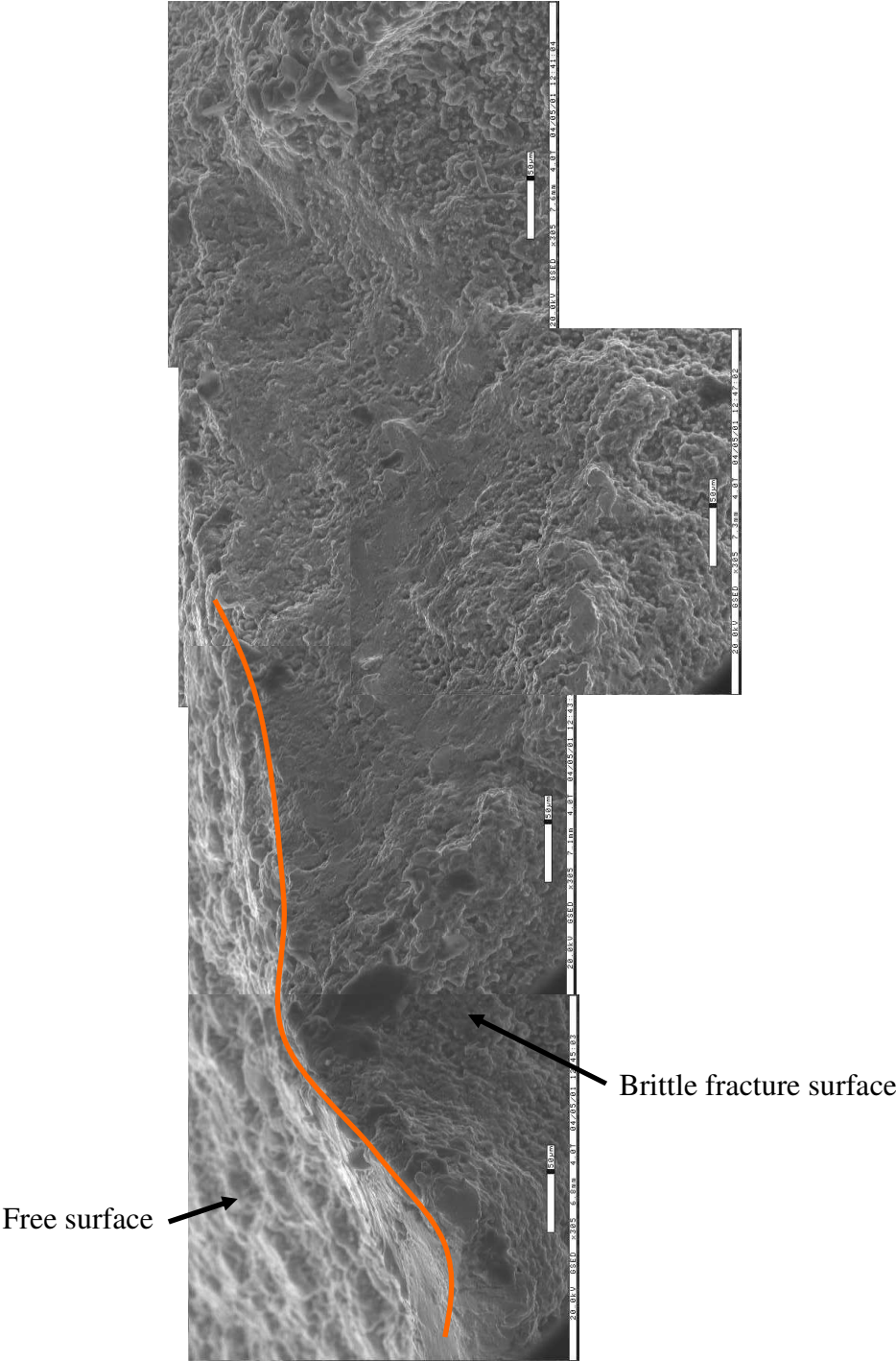


Figure 31. Image of an embrittled portion of test specimen 4 fracture surface.

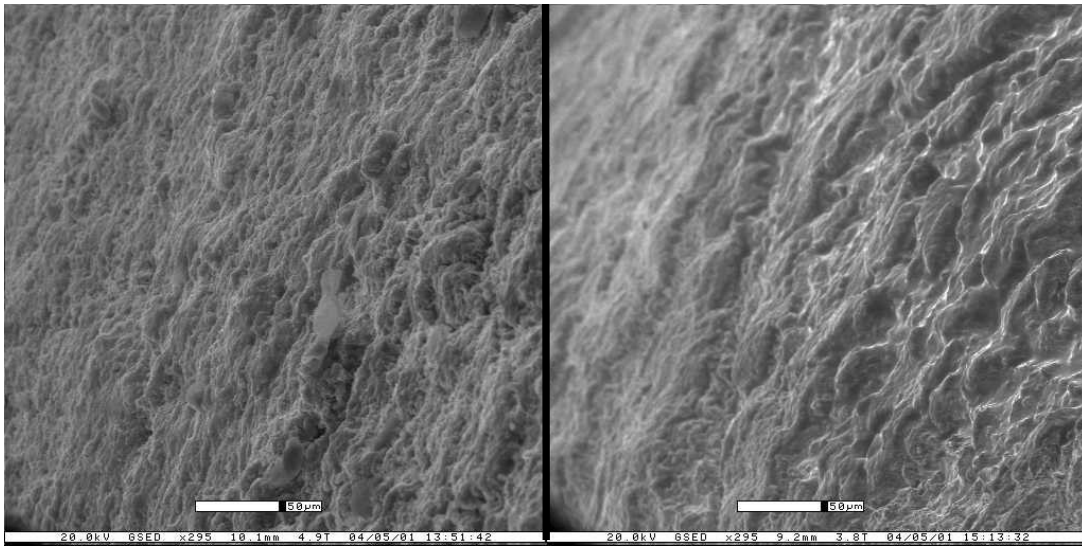


Figure 32. SEM images of test specimen 5.

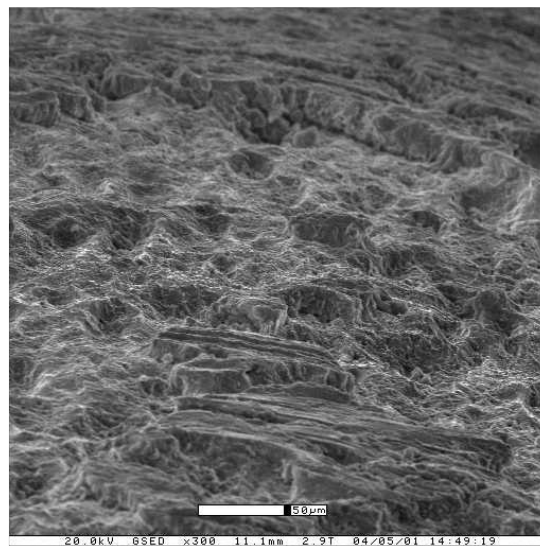


Figure 33. SEM image of test specimen 6.

The surfaces of the remaining specimens were clearly attacked by the environment, however, the presence of crack-like formations was not observed as shown in Figures 32 and 33.

All corrosion test specimen failures appeared to have initiated with MVC in the central portion of the specimen. Fast fracture occurred after the MVC area expanded and grew into a critical region that appears to have possibly been embrittled by the corrosive environment - an observation consistent with the stereomicroscopic analysis.

Energy Dispersive Spectroscopy

Energy dispersive spectroscopy (EDS) was also conducted on the fracture surfaces of the test specimens. EDS analysis was used to qualitatively determine the elements present on the surfaces. Spectra from the EDS testing and the location of the tests are shown in Figures 34 through 38. Images from the central portion of the fracture surfaces showed similar results: high iron and carbon peaks, as shown in Figures 34, 35, and 38. As shown in Figure 36, analysis of the surface of test specimen 2 revealed a significant presence of aluminum and cobalt, neither of which should be present in this particular type of steel. Aluminum is typically used as a deoxygenizing agent when the steel is killed, possibly the presence of the aluminum is a result of this process. As a whole, the presence of these other elements in significant levels is the result of poor quality. Figure 37 indicates the presence of iron and oxygen peaks, consistent with iron oxide corrosion product. Other elements present are elements in the steel or possibly the result of the environmental components.

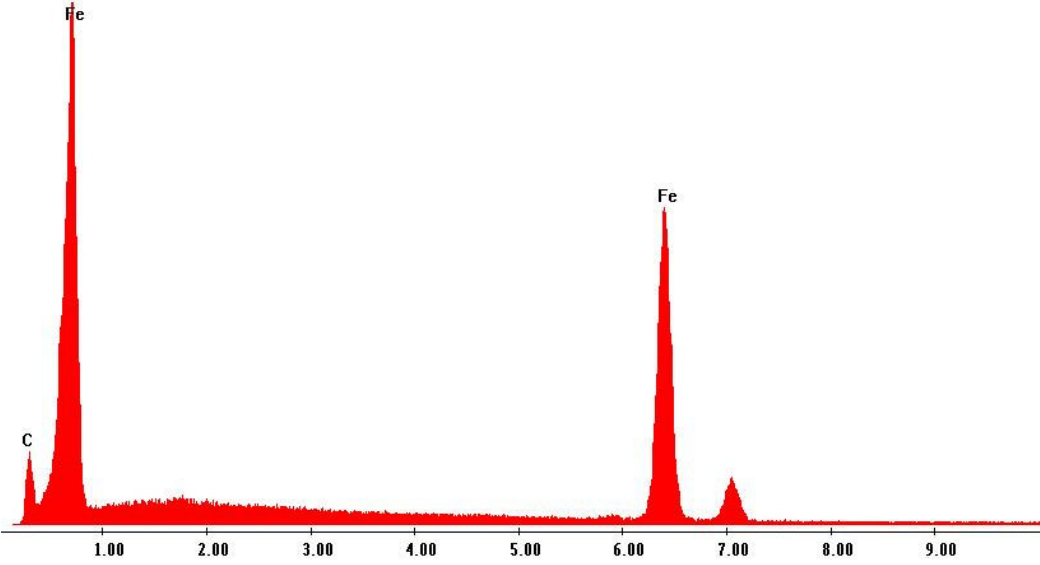
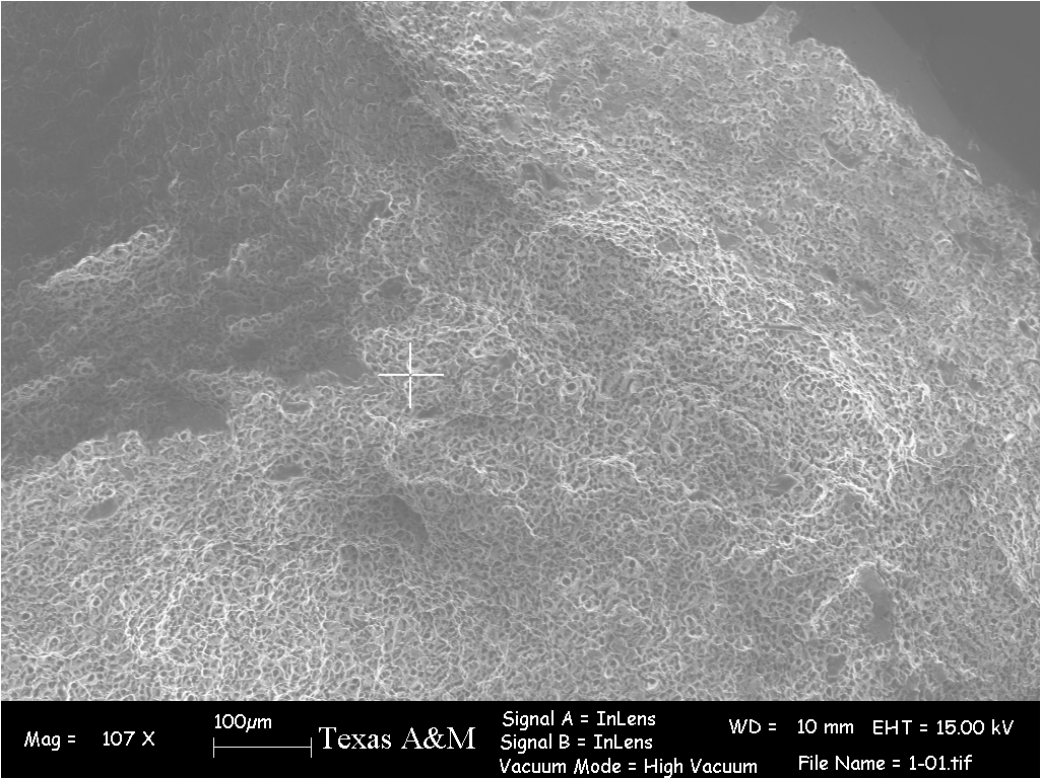


Figure 34. EDS analysis of test specimen 1.

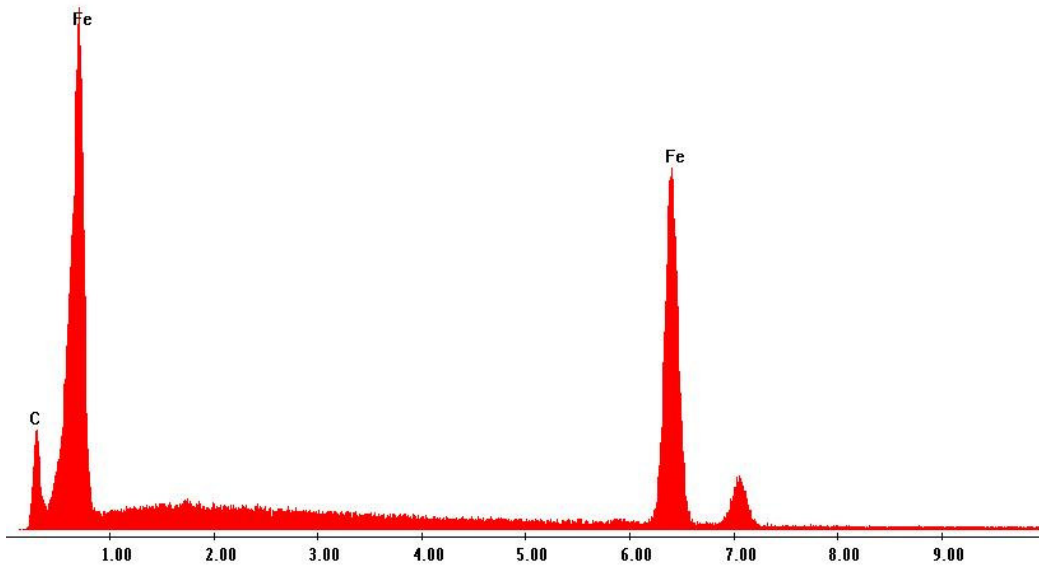
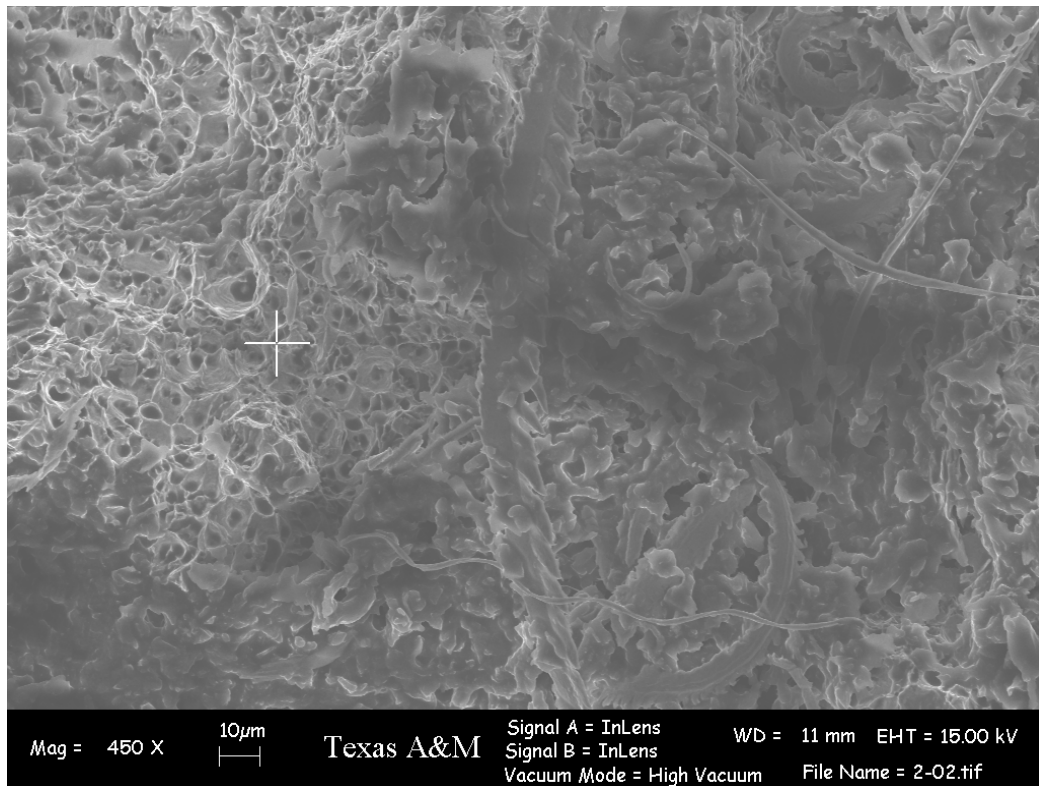


Figure 35. EDS analysis of test specimen 2.

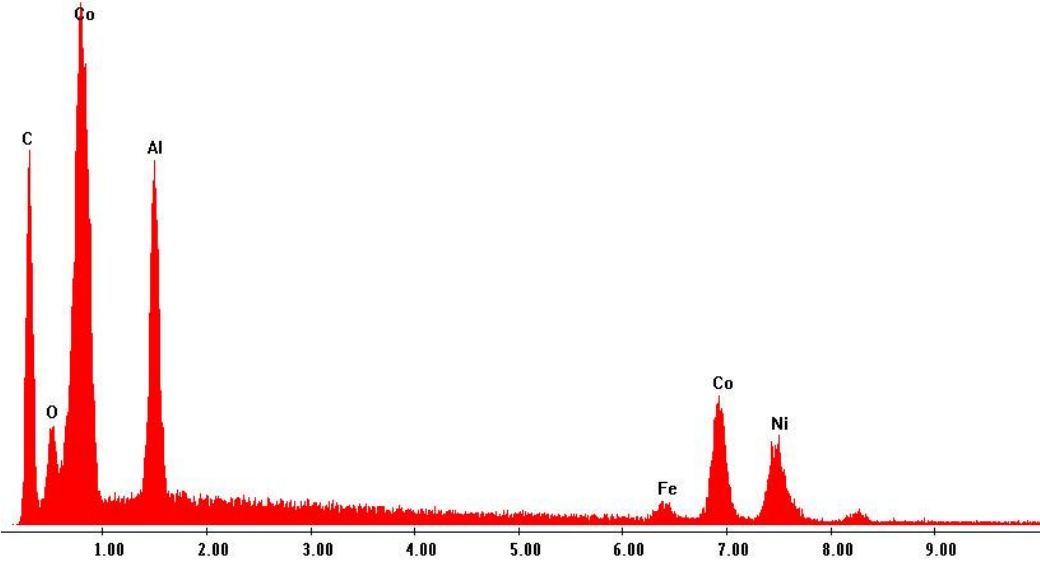
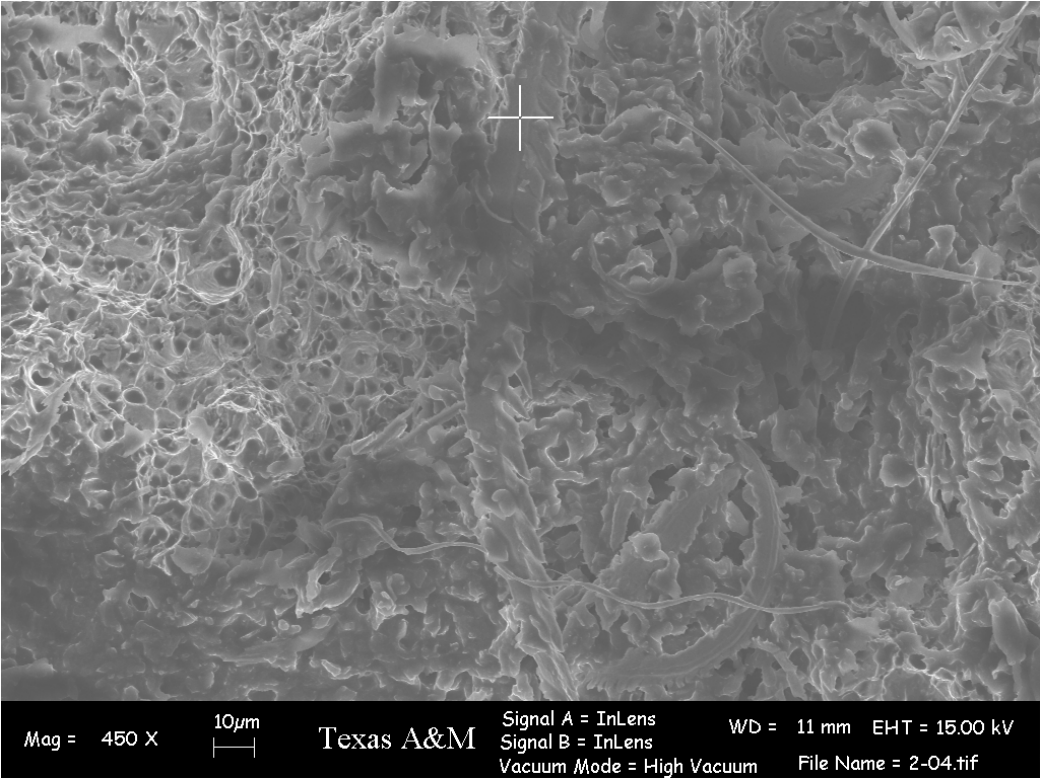


Figure 36. EDS analysis of test specimen 2 anomaly.

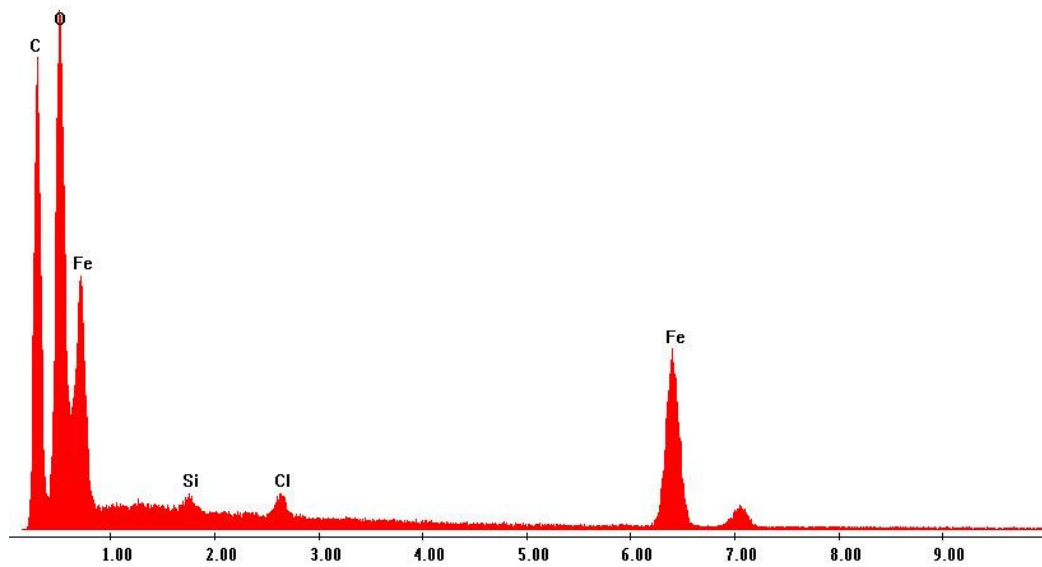
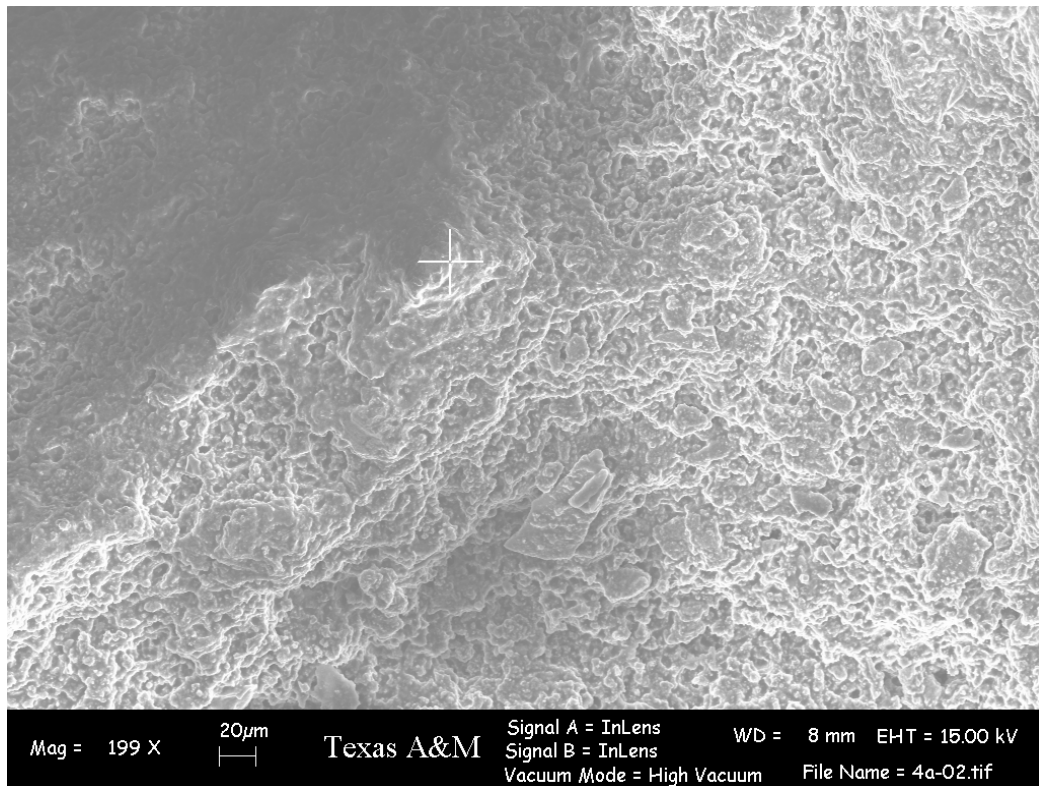


Figure 37. EDS analysis of test specimen 4 – corrosion product.

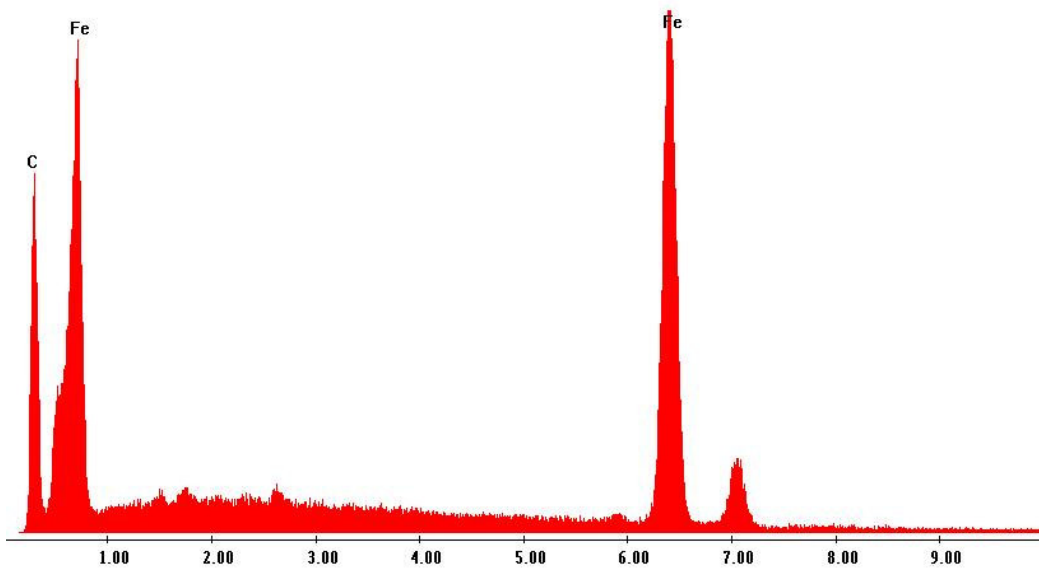
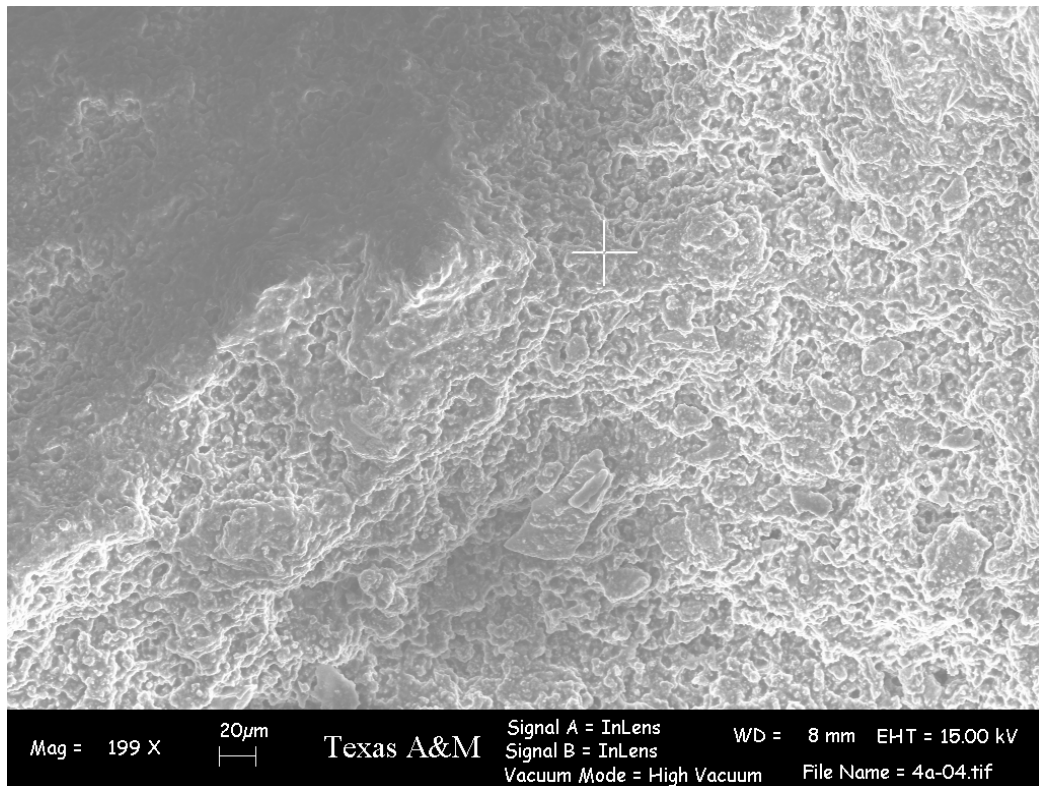


Figure 38. EDS analysis of test specimen 4 – near surface.

Metallographic Analysis

Metallographic analysis of numerous samples revealed a ferrite matrix with pearlite interspersed with what appears to be a great number of inclusions sized at roughly 0.10 mm in diameter. The composition of the particles was inconclusive, as the EDS analysis did not detect the presence of any elements other than iron and carbon in any significant level, excluding specimen 2. The orientation of the particles also did not suggest any type of directionality, as shown in Figure 39.

Pitting was evident rather than the classical "riverbranch" form of SCC. There was at least some evidence of decohesion at the surfaces between the particle and matrix interfaces – locations that possibly served as initiation sites for the larger pits ranging in depth from 0.75 to 2.00 mm. Some secondary cracking was also observed branching from the pit walls, as shown in Figure 40.

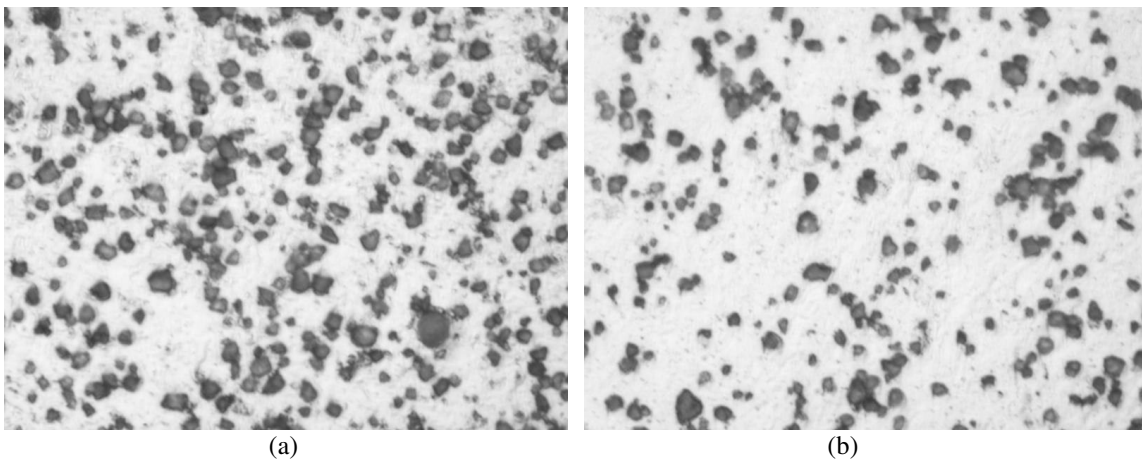
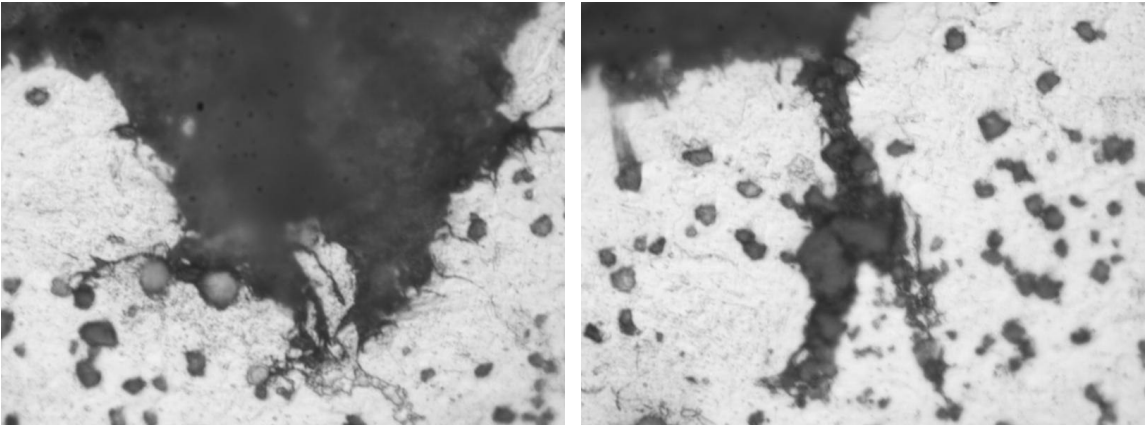
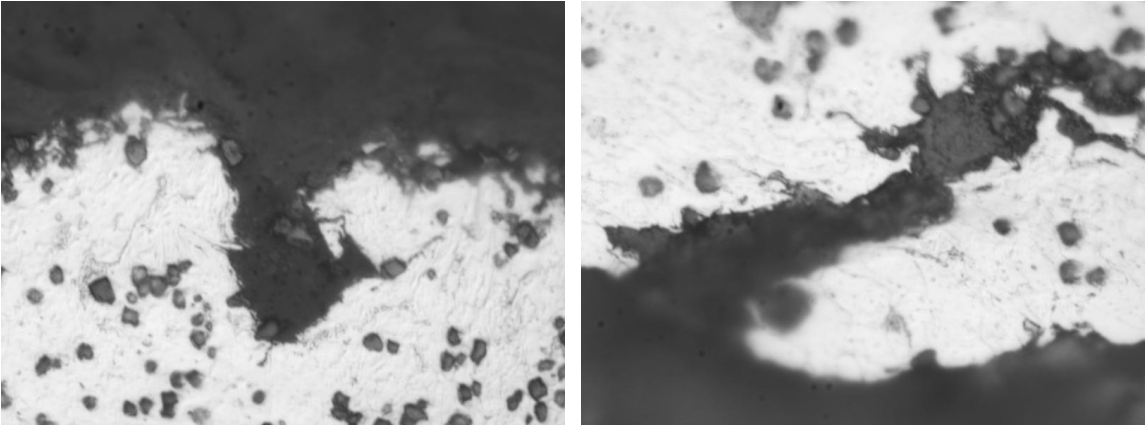


Figure 39. Micrographs from test specimens 1 and 2.

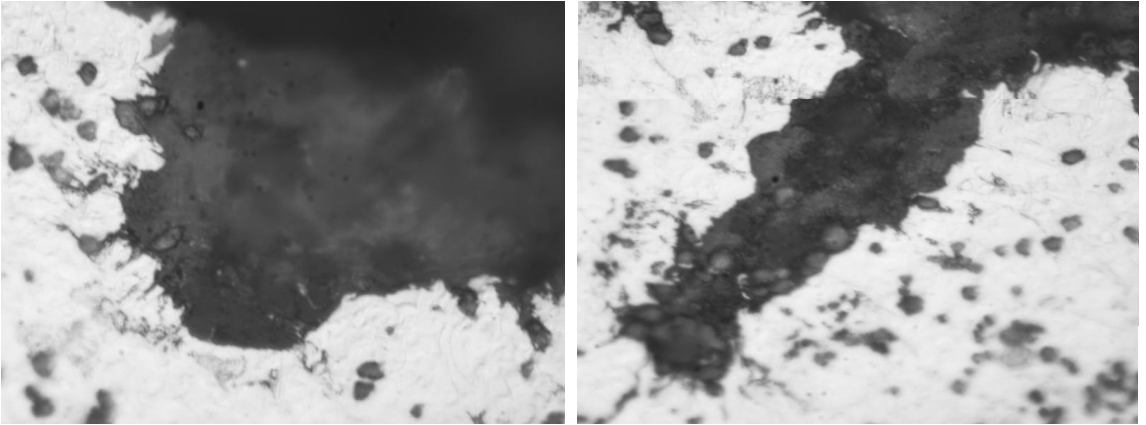
(a) Parallel to axis of pipe in specimen 1, and (b) perpendicular to axis of pipe in specimen 2.



(a)



(b)



(c)

Figure 40. Images of pits in the test specimens.
(a) Test specimen 4, (b) test specimen 5, and (c) test specimen 6.

The micrographs of the samples tested do not have the typical appearance for the structure of API 5L X-52 as shown in Figure 41. The test specimens' ultimate tensile strength, however, was appropriate when compared to the values listed in API 5L for X-52 as shown in Table 8.

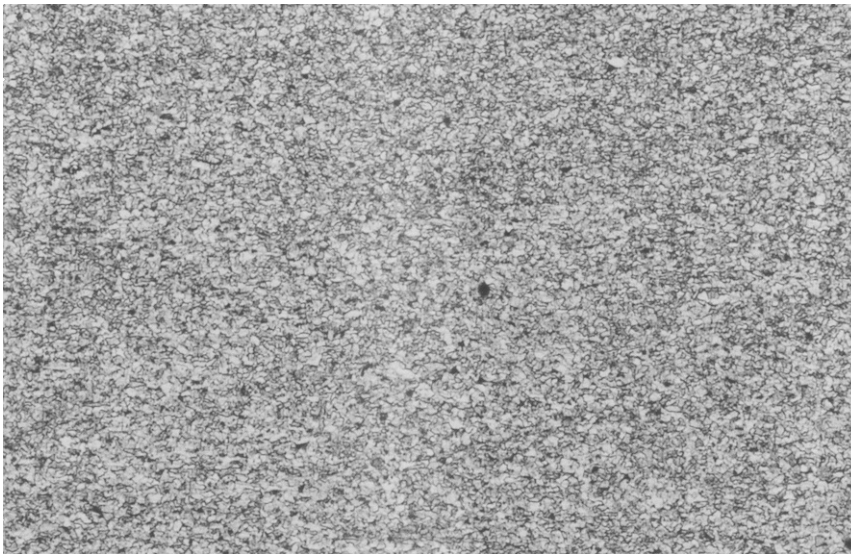


Figure 41. *Lateral section of X-52 pipeline steel (x100).*

TABLE 8

API 5L Strength Requirements

Ultimate Strength Minimum (MPa / ksi)	Ultimate Strength Maximum (MPa / ksi)
455 / 66	758 / 110

Marin Factor Analogy

Table 9 lists the ratios of the corrosive and ambient results for corresponding tests, i.e., 1 and 4, 2 and 5, 3 and 6. Each ratio was multiplied by the baseline time-to-failure for its corresponding control test, that is test 1, 2, or 3, to predict the lifetime of the specimen in the corroded environment as shown in Table 10. Table 11 then lists the root mean square variance between the predicted lifetime and the actual corrosive lifetimes. The root mean square was used to determine which set of ratios provided the least variation between predicted and actual values.

TABLE 9

Ratio of Corrosive Results and Ambient Results

Test	Ultimate Load	Fracture Load	Ultimate Stress	Fracture Stress	% Reduction in Area	% Elongation
1 & 4	0.97	0.98	0.98	0.75	0.89	0.63
2 & 5	0.96	0.91	0.96	0.84	0.97	0.90
3 & 6	0.93	0.95	0.93	0.70	0.87	1.03

TABLE 10

Test Specimen Lifetime Prediction from Ratios

Test	Ultimate Load	Fracture Load	Ultimate Stress	Fracture Stress	% Reduction in Area	% Elongation
1 & 4	11.73	11.92	11.85	9.03	10.72	7.57
2 & 5	15.93	15.03	15.93	13.92	16.11	14.97
3 & 6	39.69	40.42	39.69	29.78	37.00	43.78

TABLE 11
Root Mean Square Variance

Ultimate Load	Fracture Load	Ultimate Stress	Fracture Stress	% Reduction in Area	% Elongation
3.04	3.58	3.09	4.16	1.72	4.69

It is apparent from Table 11 that the least variance occurs when the ratio of % reduction in area is used to predict the lifetime of a specimen in the corrosive environment. Figure 42 graphically depicts the results of the prediction.

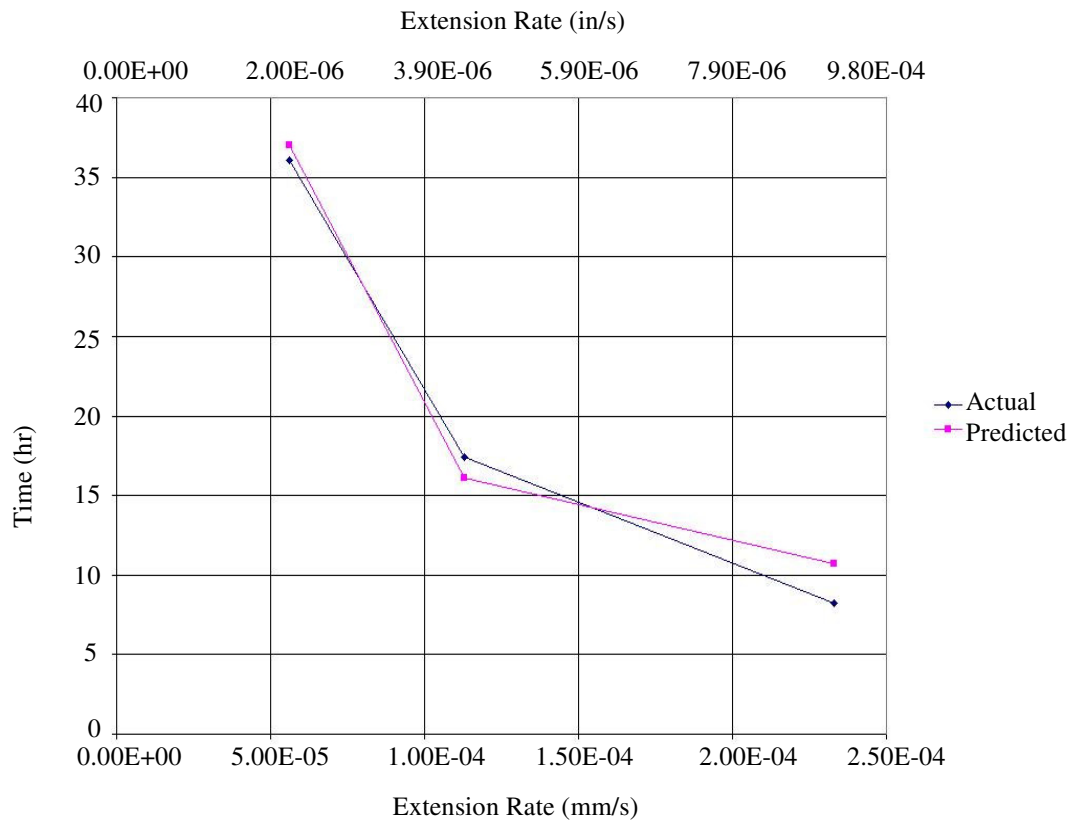


Figure 42. Prediction of specimen lifetime from reduction in area.

The fact remains, however, that numerous tests must be conducted in order to obtain the necessary ratios required to predict a lifetime. It would be much more useful if data from one set of tests could be used to predict lifetimes at other extension rates, e.g., if a ratio obtained from tests 1 and 4 could be used to predict the lifetimes of tests 2 and 5, and 3 and 6.

Currently, there are three ratios for % reduction of area, 0.89, 0.97, and 0.87 for tests 1 and 4, 2 and 5, and 3 and 6 respectively. Table 12 is obtained by multiplying each ratio by the three measured ambient lifetimes 12.10, 16.58, and 42.48 hr.

TABLE 12
Lifetime Prediction Matrix

Ratio	Lifetime		
	12.10 (Test 1)	16.58 (Test 2)	42.48 (Test 3)
0.89 (Test 1&4)	10.769	14.7562	37.8072
0.97 (Test 2&5)	11.737	16.0826	41.2056
0.87 (Test 3&6)	10.527	14.4246	36.9576

TABLE 13
Root Mean Square Variance of the Lifetime Predictions

Ratio	RMS
0.89 (Test 1&4)	2.35
0.97 (Test 2&5)	3.69
0.87 (Test 3&6)	2.23

Table 13 indicates that the ratio for % reduction of area during tests 3 and 6 has the least variance. It is suggested that this ratio could be used in Equation 10, repeated here for convenience:

$$L_C = C_1 L_A \quad (10)$$

In this case, rather, the lifetime is for the test specimen in the corrosive environment and L_A is the measured ambient lifetime at the extension rate of interest. Figure 43 depicts the lifetimes for multiple specimens utilizing 0.87, the ratio from tests 3 and 6.

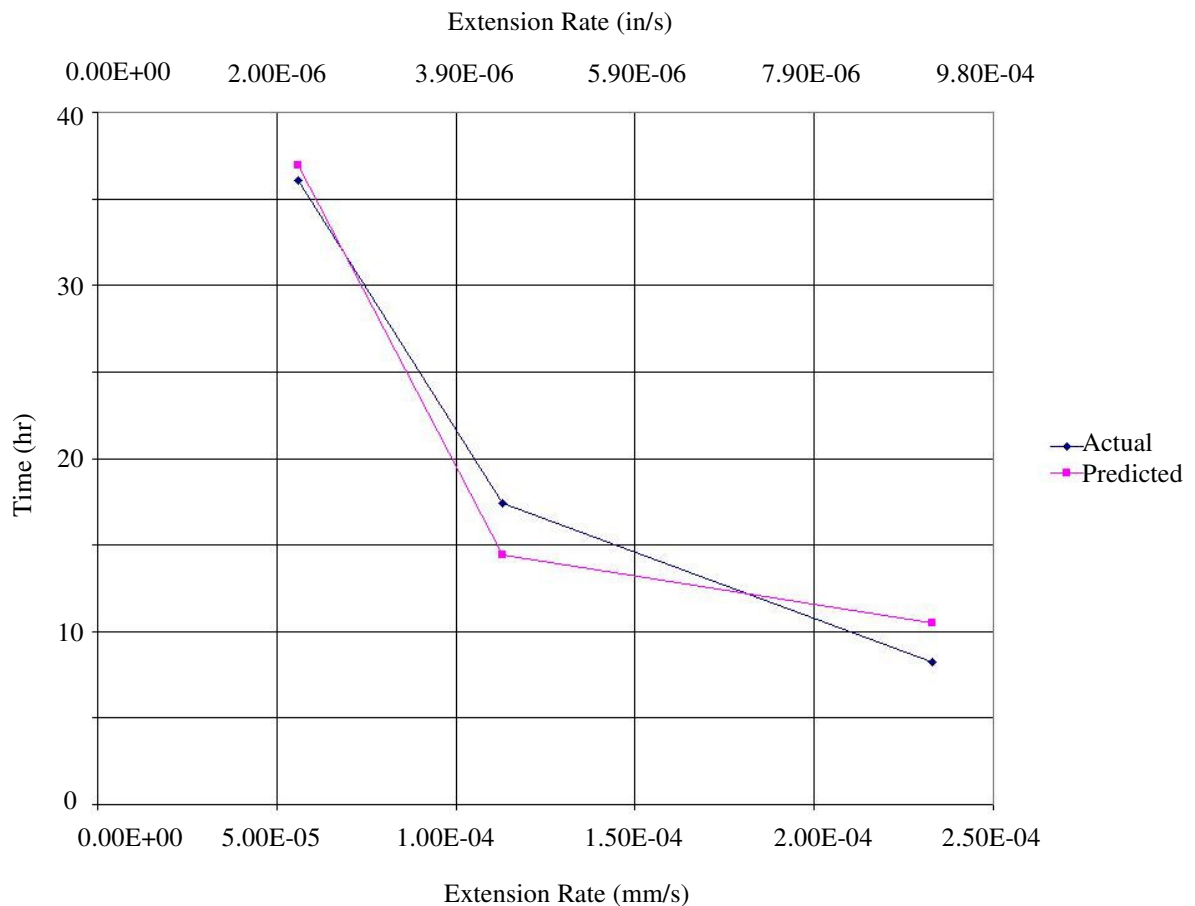


Figure 43. Graph of the generalized ratio prediction.

Although the generalized ratio prediction is in general agreement with the actual values, there is not enough information to determine the values of any subfactors, that is, the specific effects of the environment, the material, and the load. The fact remains that this could and most likely is an isolated phenomenon. Simply put, the sample size is too small for this ratio to be of any practical significance. The idea, however, of a Marin factor analogy could still be plausible. Further experimentation is needed to determine if there exists a ratio or set of ratios suitable for general use. If indeed there is a ratio, then future research could focus on the development of shape, size, and load factors to bridge the gap between test specimen and pipeline geometries - ultimately providing a tool to predict the lifetimes of damaged pipelines.

Strain Energy Concept

EAC is an inherently complicated phenomenon. The material or component may react in numerous ways to its environment and state of stress. Individual cracks may initiate, propagate, coalesce with adjacent cracks, or become dormant. Rather than trying to model each individual possibility, it may prove to be more practical to approach the development of a model from a cumulative perspective. For instance, an examination of the load / extension curves for the test specimens reveals a marked reduction in the area under the curves for the specimens tested in the corrosive environment - the area under the curve being the elastic strain energy and the plastic work.

Neglecting any elastic deformation of the test rig, the only energy input into the ambient tests occurs from the load acting through the specimen extension. Given that

the specimen geometries are identical, the effects of the corrosive environment are represented by the differences in areas between the ambient and corrosive curves as shown in Figures 44 through 46.

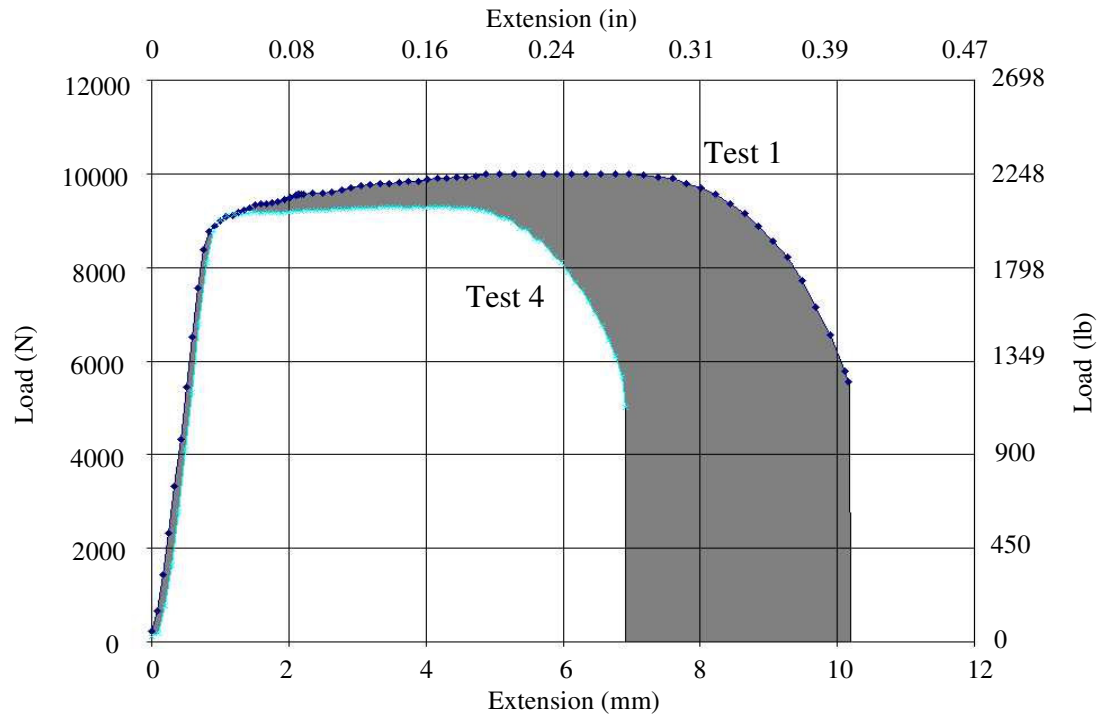


Figure 44. Graphic of the difference in energy for tests 1 and 4.

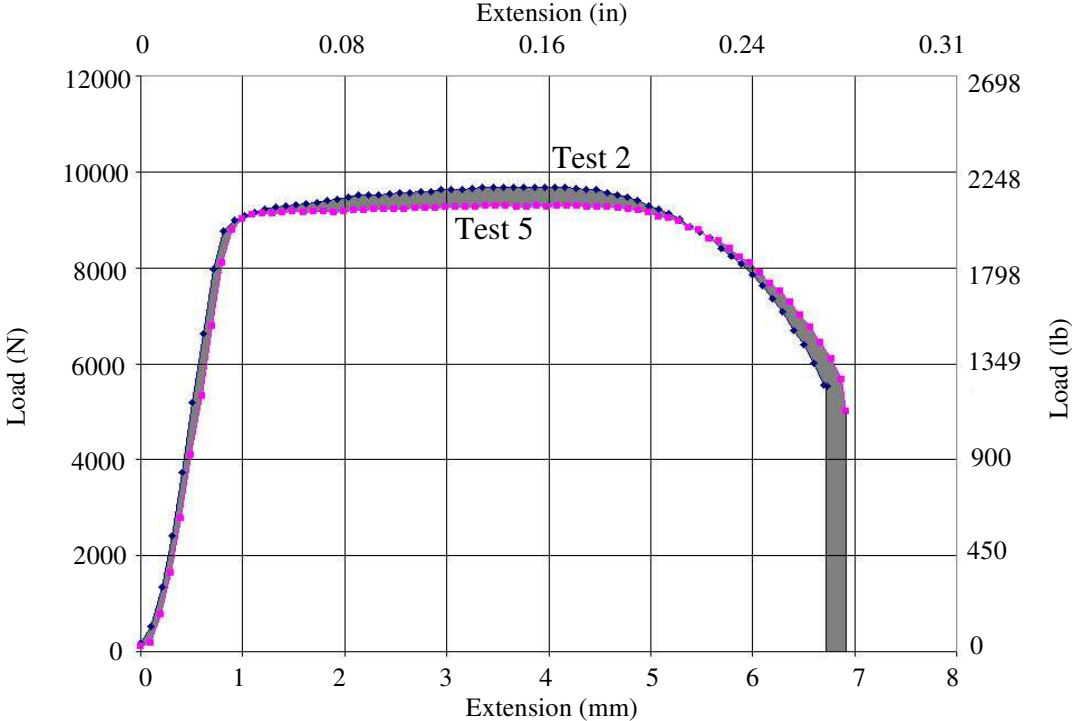


Figure 45. Graphic of the difference in energy for tests 2 and 5.

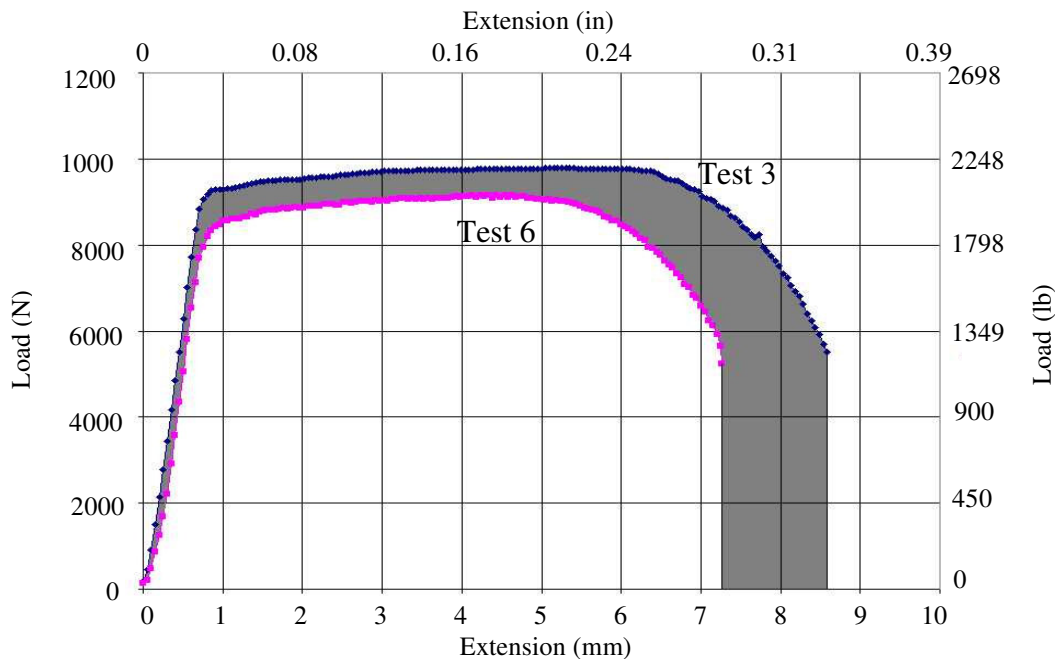


Figure 46. Graphic for the difference in energy for tests 3 and 6.

Consider tests 1 and 4. The energy that must be dissipated by the effects of the environment is known, i.e., the difference in area under the curves. The amount of time in which the energy must be dissipated is known, i.e., the time for test 4 to complete. Knowing the energy and time establishes the rate at which energy must be dissipated from the system.

In reality the test specimens experience plastic deformation and the principles of linear elastic fracture mechanics are probably not the most suitable for describing their behavior. The J-integral might prove to be more appropriate for modeling the actual test specimen behavior. In the pursuit of simplicity, it can be assumed that there is small scale yielding in the model in which case the J-integral becomes equal to G – the strain

energy release rate given by dU/dA , where U is energy and A is the crack area.

Considering average values then the following relationship exists:

$$\Delta U/\Delta t = (\Delta U/\Delta A) (\Delta A/\Delta t) \quad (12)$$

If $\Delta U/\Delta t$ is known and a crack geometry is assumed then $\Delta U/\Delta A$ is established.

Knowing $\Delta U/\Delta t$ and $\Delta U/\Delta A$ then allows the determination of $\Delta A/\Delta t$ – the crack growth rate. In essence, this is a model that represents the cumulative effects of the corrosive environment as a crack with the same average energetic properties. From this model we can extract a growth rate $\Delta A/\Delta t$ which can be manipulated to provide a penetration rate. A problem arises, however, because the strain energy release rate increases as the crack grows, therefore an average value for G will most likely not give an accurate depiction of the penetration of the crack. In this case it is necessary to know G at each instant of crack propagation.

From the data collected in the CERT experiments there is no way to determine how the strain energy released during crack propagation might be distributed. For instance, the total energy to be dissipated is known and the difference in energy between tests 1 and 4 can be expressed as a function of extension rate, but this function has no meaning when applied in the model which only exists for the duration of test 4. The difference in energies occurring after the end of test 4 must be redistributed according to some currently unknown function. Although the concept is somewhat under developed, it does suggest that future research based on the energy method may provide a cumulative means of quantifying the effects of EAC.

APPLICATION TO PIPELINE LIFETIME AND FUTURE RESEARCH

When corrosion is found in a pipeline there is a need for a method of determining the remaining strength and lifetime of the corroded areas. Therefore one of the needs of industry has been a method that will assist operators in determining whether a section of pipeline should be repaired or replaced. A considerable hurdle has been the extensive testing and research necessary to develop the knowledge base required for the development of accurate and safe models. Currently, ASME B31G “Manual for Determining the Remaining Strength of Corroded Pipelines” is only suitable for use with defects having smooth contours, i.e., pits and not any form of cracking. The research and ideas expressed in this thesis represent an effort to assist in the development of knowledge necessary in the determination of the remaining lifetime of pipelines subject to EAC.

A primary limitation of this study has been the small data set; three sets of tests simply do not produce enough results to be industrially practical. The small amount of data can in no way be directly applied to any field situations. In order for the ideas to be developed further more tests must be conducted. The tests should include a broader range of extension rates as well as other environments, i.e., different concentrations of species, temperatures, and solution pH values. In the future, test specimens may also need to be polished to reduce the influence of the fabrication process. It would be beneficial to conduct tests on various grades of pipeline steel and in turn similar steels of various qualities. As such, future research will need to include pre-test chemical analysis and metallography to verify the specific type of material and its quality. The

results from a significant number of tests could be used to further develop the model based on the Marin factor analogy. In the interest of saving time and resources it may also be more efficient to use test specimen geometries that have been used by larger commercial research enterprises so that information can be exchanged.

The leap from test specimen to pipeline is of significant importance. A correlation between the two will have to be developed. The American Gas Association (AGA) and the Pipeline Research Committee International (PRCI) have constructed a database with information from over 250 pipeline burst tests. This information could prove beneficial in the development of size and shape factors in the Marin analogy. The size factor should account for the fact that ERW pipe is formed from flat strip into a circular cylinder and as such pipes of smaller diameter will experience a greater level of strain during the rolling process.

At current, the energy method is nothing more than a concept. The energy method model needs further development to be used as a predictive tool and applied to pipelines in the field. Future research could possibly include more fracture mechanics oriented test specimens to increase the scope of the data available for the model. It may be of particular interest to perform J-integral testing with precracked specimens. Battelle also has finite element analysis (FEA) software entitled PCORR that may assist in expanding the energy method concept. As a matter of convenience, test specimen geometries should be such that conditions of plain strain or plane stress exist. As mentioned previously, relationships between different environments, materials, extension rates, sizes, and shapes will need to be determined as well.

CONCLUSION

Results from the constant extension rate tests indicated that the simulated groundwater solution and applied potential decreased the ductility of each of the test specimens. An inspection of the load / extension curves for the corroded specimens revealed that the modulus of toughness was generally lower than that of the ambient specimens. Fracture stress for the corroded specimens was also reduced by 16% - 30%.

Stereomicroscopic analysis of the corroded test specimens revealed fracture surfaces consistent with failures of a primarily ductile nature. The presence of flat, shiny plateaus around some of the fracture surfaces suggested that the corrosive environment affected the metal near the free surface exposed to the groundwater simulation solution. SEM analysis further confirmed the existence of areas appearing to have failed in a brittle manner. Subsequent metallographic analysis revealed the presence of corrosion pits rather than “river branch” cracks typically observed with SCC. Separation between the ferrite and what appeared to be numerous inclusions was also visible near the surfaces and could have served as initiation sites for the corrosion pits. No evidence of classical SCC morphology was discovered although the pits did have some traces of secondary cracking.

The concept of a Marin factor analysis was explored and the ratio of % reduction in area was used to predict the lifetime of samples tested at various extension rates. An energy method model was then suggested through comparison of the load / extension curves for each set of tests. In essence, this concept suggests that a geometric crack could be used to model the cumulative effects of the corrosive environment.

The number of samples tested was too small to generate any immediately applicable models. Future research will need to focus on the generation and collection of a great deal of additional data. Subsequent testing should focus on the effects of multiple environments, materials, and loading conditions. In addition, size and shape factors need to be determined in order to achieve the transition from test specimen geometry to a pipeline geometry.

REFERENCES

1. Research and Special Programs Administration, "Pipeline Statistics," Office of Pipeline Safety, <http://ops.dot.gov/stats.htm> (Nov. 11, 2003).
2. J.L. Kennedy, Oil and Gas Pipeline Fundamentals, Tulsa, OK, PennWell, 1993.
3. A. Priambudi, "Lifetime Prediction of Pressurized Pipelines in Corrosive Environments," Master's technical report, Texas A&M University, 2001.
4. R.J. Landrum, Fundamentals of Designing for Corrosion Control – A Corrosion Aid for the Designer, Houston, TX, NACE, 1989.
5. D.A. Jones, Principles and Prevention of Corrosion, Upper Saddle River, NJ, Prentice-Hall, 1996.
6. W. Zheng, R. Sutherby, R.W. Revie, W.R. Tyson, G. Shen, "Stress Corrosion Cracking of Linepipe Steels in Near-Neutral pH Environment," Corrosion Engineering, http://64.224.111.143/corrosioneering/journal/Jul02_Revie/Jul02_Revie_1.htm (Oct. 4, 2003).
7. A. Teitsma, "Gas-Coupled Ultrasonic Inspection of Pipelines," Pipeline and Gas Journal, www.pipelineandgasjournal.com (Sep. 12, 2003).
8. ASM Handbook, Vol. 11: Failure Analysis and Prevention, 10th ed., Materials Park, OH, ASM International, 2002.
9. R.N. Parkins, "The Controlling Parameters in Stress-Corrosion Cracking," Proc. 5th Symposium on Line Pipe Research, Arlington, VA, AGA, 1974, U-1.

10. T.M. Devine, Jr., G.S. Frankel, R.H. Jones, R.G. Kelly, R.M. Latanision, J.H. Payer, "Final Report Waste Package Materials Performance Peer Review Panel," Office of Civilian Radioactive Waste Management, http://www.ymp.gov/documents/peer_rev/index.htm (Feb. 2, 2004).
11. F.P. Ford, "Status of Research on Environmentally-Assisted Cracking in LWR Pressure-Vessel Steels," Proc. 5th National Congress on Pressure-Vessels and Piping Technology, San Diego, CA, AIME, 1987.
12. B. N. Leis, R. N. Parkins, *Fatigue and Fracture of Engineering Materials and Structures* 21 (1998) 583-601.
13. R. N. Parkins, *Corrosion* 43 (1987) 130-139
14. R.N. Parkins, *Corros. Sci.* 20 (1980) 147-166.
15. R.N. Parkins, "Overview of Intergranular Stress Corrosion Cracking Research Activities," PRCI, Final Report PR-232-9401, Houston, TX, PRCI, 1994.
16. R.L. Wenk, "Field Investigation of Stress-Corrosion Cracking," Proc. 5th Symposium on Line Pipe Research, Arlington, VA, AGA, 1974, T1-T22.
17. A. Turnbull, *Corros. Sci.* 34, 6 (1993) 921-960.
18. H. Leidheiser, Jr., R.D. Granata, G. Fey, M. Ingle, *Corros. Sci.* 28, 6 (1988) 631-632.
19. Y.S. Garud, A.R. McIlree, *Corrosion* 42, 2 (1986) 100.
20. X.Y. Zhang, S.B. Lambert, A. Plumtree, *Corrosion* 55, 3 (1999) 299.

APPENDIX A**PIPELINE CHEMICAL AND MECHANICAL INFORMATION**

02/10/2004

CERTIFICATE OF TESTS

Heat Number	Item Number	DESCRIPTION
133256	P1526280BDRLP	API5L X52 6-5/8"X.280" WALL(18.99#) BARE,DRL,PEB

CHEMICAL ANALYSIS

	C	Mn	P	S	Ni	Cr	Cu	Mo	Si	Al	V	Nb	B	Ca	CE
Ladle-	0.050	0.720	0.010	0.004	0.004	0.011	0.014	0.001	0.117	0.023	0.001	0.020	0.0001	0.0020	
Chem -	0.071	0.700	0.008	0.006	0.010	0.014	0.022	0.006	0.132	0.028	0.002	0.017	0.0005	0.0028	.12
Chem -	0.071	0.700	0.008	0.007	0.011	0.014	0.022	0.006	0.134	0.028	0.001	0.017	0.0002	0.0030	.11

MECHANICAL PROPERTIES:

YS(ksi): 61.6 TS(ksi): 69.3 EL(%): 33% HRB: 87 Y/T(%): 0.89

COMMENTS

HYDROSTATIC TEST PRESSURE (psi): 3,000 FOR 5 SECONDS

MANUFACTURED TO THE 42ND EDITION OF API 5L SPECIFICATION
MANUFACTURED IN THE U.S.A.

ELECTRIC RESISTANCE WELDED PRODUCT
WELD SEAM ANNEALING AT 1500 DEGREES F. MINIMUM

ULTRASONIC AND ELECTROMAGNETIC TESTING (N-10 NOTCH, 1/8" DRILLED HOLE)
FLATTENING TEST PASSED
1 INCH STRIP SPECIMEN.

THIS MATERIAL MEETS: ASTM A53B, ASME SA53B
PSL1 - API 5L, GRADES B, X42, X46, X52
PSL2 - API 5L, GRADE X42,X52

MEETS NACE STANDARD MR0175
STANDARDS ARE LATEST REVISION

FOR REFERENCE ONLY
Document Cont

The above analyses and tensile properties are correct
to the best of my knowledge and belief.

Quality Control Dept

Figure 47. Material chemistry data

CS TECHNITRADE
 L.O. 4511 BRITTMORE RD
 HOUSTON, TEXAS 77041
 N T
 E O

HOUSTON, TEXAS
 D S
 T P
 I N T
 O O

OCOMPRA - Purchase Ord. N° NET 120 DAYS
 OVENTA - RN - Sider Ord. N° SA7777B -04
 DESPACHO - Shipper N°
 FACTURA - Invoice N°
 VEHICULO - Vehicle CUMBRIAN EXPRESS
 LOTE: L0001

PRODUCTO Product
 HOT ROLLED STEEL COILS.

SIZE
 0.2740 " NOM X 41.300 "

COLOUR MARK

TIPO DE ANALISIS Analysis Type
 HEAT PHYSICAL TEST

N° COLADA Heat N°
 MIN. MAX.

CHEMICAL COMPOSITION - %

N° MUESTRA Sample Identification	ESF Y.P. MPA	ESF UTS % AL	TRADICION	IMPACTO	DOB S. GR	CHEMICAL COMPOSITION - %									
						V	NI	CR	B	N	TI	CA			
132856	411,00	473,00	35,00	890	OK	010	020	001	006	010	000	003	002	020	
132859	401,00	469,00	42,00	810	OK	010	001	001	011	000	003	002	020	020	
133256	372,00	475,00	41,00	2000	OK	009	020	001	004	011	001	004	001	020	
133257	423,00	478,00	38,00	2210	OK	010	020	001	022	011	001	004	001	020	
133258	399,00	463,00	37,00	2040	OK	010	020	001	006	005	001	004	001	020	
231043	418,00	490,00	35,00	1890	OK	010	023	001	004	014	001	006	001	020	
433225	361,00	459,00	37,00	700	OK	010	021	001	015	014	001	004	001	020	
433226	376,00	457,00	41,00	880	OK	010	020	002	005	014	001	003	002	020	
433576	400,00	464,00	37,00	1960	OK	010	021	001	005	011	001	004	001	020	
433580	397,00	465,00	40,00	1920	OK	010	019	001	001	007	001	004	001	020	

FOR REFERENCE ONLY
 Document Control

Figure 48. Material mechanical data.

APPENDIX B

TEST MACHINE CALIBRATION DATA

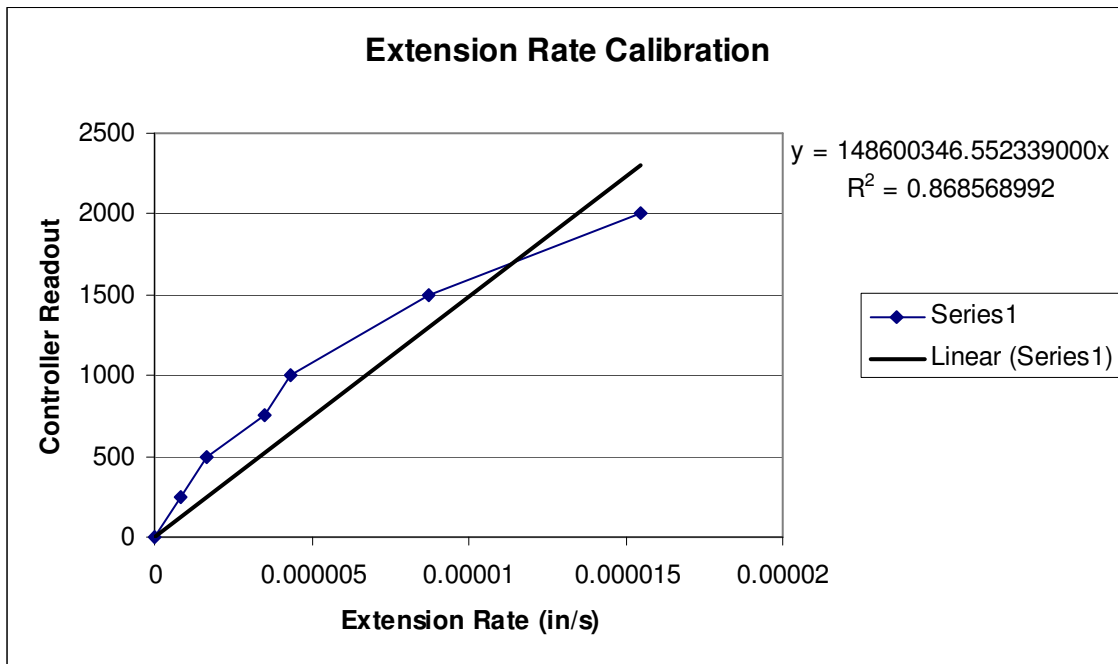


Figure 49. Graph of calibration data.

The trendline was used to set the crosshead speeds for all tests. Note that the dimensions for this particular figure are English.

VITA

Jason Wayne Curbo

Permanent Address

601 Enterprise Avenue #228

League City, TX 77573

Educational Background

Bachelor of Science in Mechanical Engineering University of Arkansas May 1999

Master of Science in Mechanical Engineering Texas A&M University May 2005

Work Experience

ExxonMobil Chemical Company, Baytown, Texas
Mechanical Engineer – Pyrolysis March 2004 - Present

Department of Mechanical Engineering, Texas A&M University
Research Assistant, September 2003 – December 2003

Department of Mechanical Engineering, Texas A&M University
Teaching Assistant, September 2002 – August 2003

Domtar Industries Incorporated, Ashdown, Arkansas
Mechanical Project Engineer, August 2001 – August 2002

Georgia-Pacific Corporation, Ashdown, Arkansas
Mechanical Project Engineer, November 1999 – August 2001

Black & Veatch Corporation, Overland Park, Kansas
Process & Power Mechanical Equipment Engineer, May 1999 – October 1999